Bio-nanopatterning of Titanium by Electron Beam Lithography

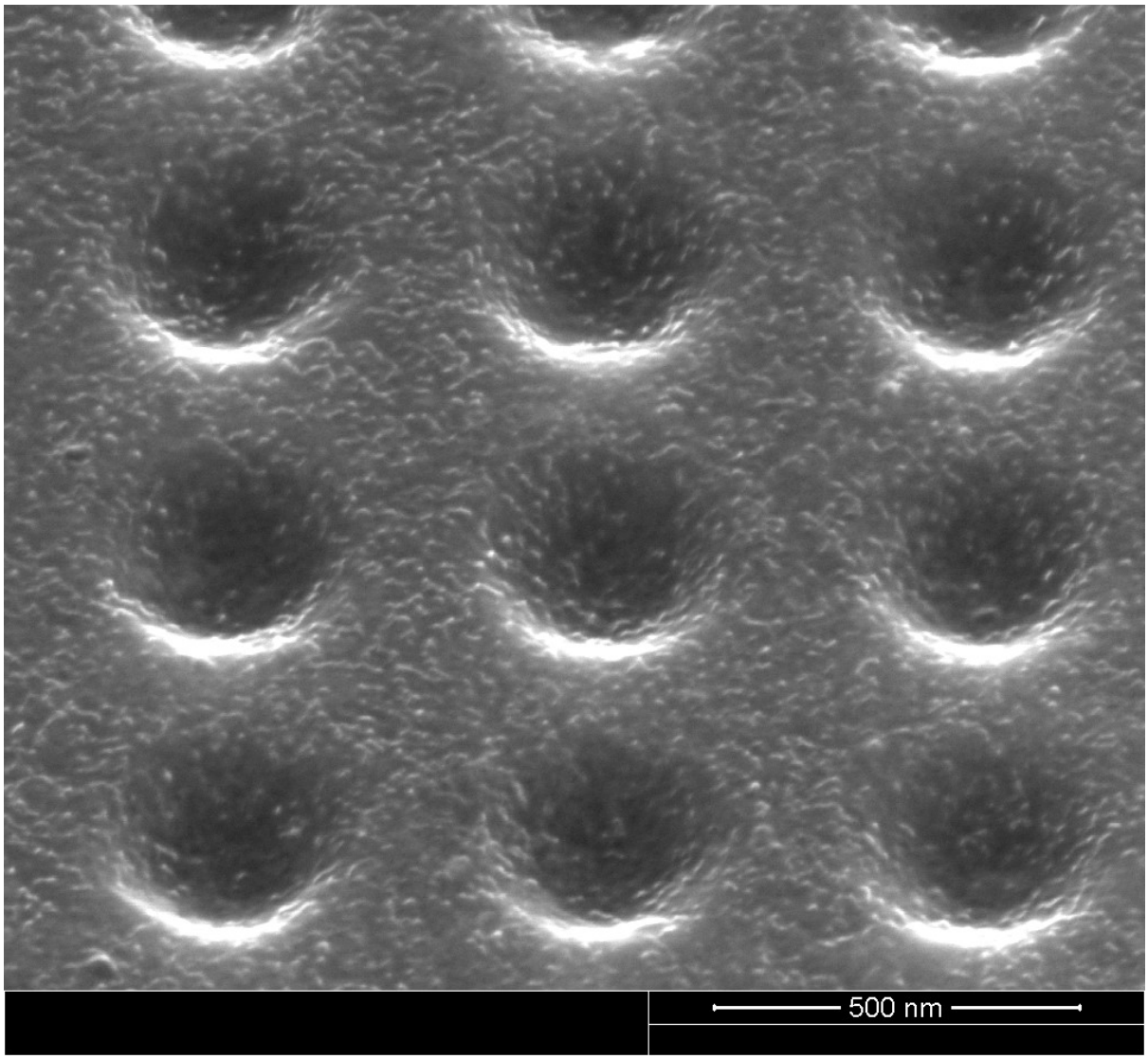

Titanium nanopits produced by the electron beam lithography method described in the thesis.

C.P.W. Hammann – 1356593
Master Thesis
Delft University of Technology
Faculty of Mechanical, Maritime and Materials Engineering
MSc. Biomedical Engineering
Specialization: Tissue Biomechanics and Implants
July 15, 2016

Supervisors: Dr. Ir. E.L. Fratila-Apachitei
Dr. C.W. Hagen
Dr. A.A. Zadpoor

TU Delft

Abstract

There is a need for joint replacing implants due to osteoarthritis and trauma. For non-cemented implants made of titanium alloys, bone ingrowth is needed. However bone ingrowth is not always accomplished. Implant micro/nanotopography can be used to enhance bone ingrowth through cellular interactions. Therefore, processes to generate controlled topographies on titanium substrates are needed. The goal of this study has been to develop a method for patterning titanium in the submicron to nanoscale. The desired patterns included pits and pillars with diameters between 30 and 700 nm, a disorder (deviation from the square arrangement in a random direction) of 0 to 75 nm, and an interspacing of 300 nm and 900 nm. To achieve this goal, the electron beam lithography process has been explored. With this process, an electron beam is used to write the pattern on the resist-coated titanium substrate. Then, the pattern is transferred into the titanium. The optimum dose for writing the patterns on the positive and negative resists has been determined experimentally. For pattern transfer, reactive ion etching, and ion milling were used, either directly onto the resist mask, or through a hard mask. The resultant topographies have been evaluated by scanning electron microscopy. The results of this study indicate that the use of hard mask, in combination with the optimum dose, and reactive ion etching conditions, generates titanium pits with 320 nm and 700 nm diameter. For pillars, further optimization of the process steps is needed. With the resist mask and ion milling, pillars of 245 nm and 545 nm in diameter with heights of 50 nm and 100 nm respectively could be obtained. In this study, a new electron beam lithography process has been developed for patterning titanium in the submicron to nanoscale. The process offers control of pattern features in these scales, this enables easy change in pattern design, and ensures pattern transfer into titanium. Therefore, the processes are considered feasible for generating patterns relevant for guiding mesenchymal stem cell fate. Previous research offered precision control into polymers, or patterns with less control into titanium.

List of abbreviations

BSS	Beam step size
d_{spot}	Spot diameter
EBL	Electron beam lithography
HMDS	Hexamethyldisilazane
MSC	Mesenchymal stem cell
OCN	Osteocalcin
OPN	Osteopontin
PMMA	Polymethymethacrylate
PSF	Approximation of the scattering effects
RF	Radio frequency
RIE	Reactive ion etching
SEM	Scanning electron microscope
α	Forward scattering
β	Backscattering
η	The ratio of the backscattered energy to the forward scattered energy

Table of contents

1 Introduction

There is a need for joint replacing implants due to osteoarthritis and trauma. Joint replacing implants are either cemented into bone or non-cemented. The non-cemented implants are made from titanium alloys, and rely on bone ingrowth. However, this bone ingrowth is not always accomplished.

The cells responsible for bone ingrowth are mesenchymal stem cells (MSCs), adult stem cells. These MSCs can differentiate into various types of cells, including osteoblasts [1]. Osteoblasts are bone forming cells.

It has been known for a long time that cells respond to their surroundings, the extracellular matrix [2]. In the case of the implant-cell interface, the topography of the implant on micro and nanoscale can direct MSC behaviour. However, it is not yet known why, and to what specific topographical cues MSCs react. This leads to the problem of understanding the cause-effect relationships between biomaterials topography and cell response.

Although it has been known that cells respond to micro and nanoscale topography, it would take until 1997 [3] to use micro/nanotopography to determine endothelial cell fate. However, it would take until 2002 [4,5] to study pattern induced differentiation for the determination of cell fate.

During literature research, multiple studies were found on the use of micro/nanotopography to induce osteogenic differentiation. The articles selected during literature research, are all without the use of osteogenic media. Several different methods were found to create a pattern to induce osteogenic differentiation: optical lithography [6-10], electron beam lithography (EBL) [11-15], through mask anodization [16,17], colloidal lithography [18,19,20], and micro/nanoimprint [6,8,13,14,18]. For these methods, also advantages and disadvantages were found during literature research. These advantages and disadvantages are summarised in Table 1.

Most promising research for guiding MSCs towards osteogenic differentiation, is performed by Dalby et al. [12]. The optimal topography defined during this study consists of pits that are 120 nm in diameter, with an interspacing of 300 nm, a depth of 100 nm, and a disorder of 50 nm from square position. The total patterned area was 1 cm^2. These patterns were created into polymethymethacrylate (PMMA) by EBL and transferred onto a nickel mould. This mould was then used for micro/nanoimprint into PMMA. The patterns created during this research guided the MSCs towards osteogenic differentiation. However, the patterns used during this research were created into PMMA.

During follow-up research of Gadegaard et al. [13], the optimal pattern for osteogenic differentiation was determined. However, the topography interspacing variable is missing during this research, and again PMMA was used as a substrate. To move towards the clinical solution for the optimal pattern, micro/nanoimprint was developed on commercially pure titanium by Greer et al. [21,22]. This nanotopography is imprinted in titanium, but the transfer is not very good.

To study the cause-effect relationships of the patterns regarding cell differentiation, it is needed to use a patterning method that can pattern features smaller than 1 µm, on titanium substrates, providing a controlled feature size, versatility in shape and spatial organization, and is reproducible. From the various methods (Table 1) EBL is a suitable method for this pattern size. Although EBL is a suitable method for these pattern sizes, there is not yet a known process to pattern the small topography into titanium.

Table 1: Advantages and disadvantages of the patterning methods, obtained from literature research.

Method	Advantages	Disadvantages
Optical Lithography	- Fast process - Larger area - Reproducible - Many shapes and sizes - Metal and polymer	- Resolution ~0.5 µm - Need a different mask for each different pattern
Electron Beam Lithography	- High resolution ~5 nm - Many shapes and sizes - Reproducible - Metal and polymer	- Slow process - Relatively small area
Through Mask Anodization	- Relatively good resolution - Fast process - Large area - Metal	- No control over shape - Hard to control size - Not exactly reproducible
Colloidal Lithography	- Relatively fast - All sizes of particles can be used (up to ~5 nm) - Metal and polymer	- No complete control over particle position - Can only use spherical particles
Micro/nanoimprint	- Resolution ~25 nm - Fast process - Larger area - Reproducible - Metal and polymer	- Need for a mother-mould - Need new mother-mould when changing shape or size - Metal very difficult

The future challenges found during literature research, lead towards research that has to be performed for the clinical application of the micro/nanotopography onto existing implant surfaces. One of the challenges found is to increase the patterned area. This means that the patterned area needs to be enlarged to implant size. Up to now only small areas (max 1x1 cm^2) are used. The patterns need to be transferred from polymers into titanium, since most studies use polymers for patterning. Also the patterns created, are mostly on flat surfaces. To move towards the clinical application curved surfaces should be considered, like Greer et al. [21,22] only with more topographical control. Finally, an application towards three dimensional patterning should be made, to incorporate the micro/nanotopography on to existing implant surfaces. A possible future application of the nanotopography onto the implant surface can be seen in Figure 1.

These future challenges have not yet been studied. Up to now, only patterns with little control have been patterned into titanium [16-20], and small patterns with great control only have been patterned into polymers [11-15].

This leads to the goal of this study: to develop an EBL process for generating submicron/nanoscale patterns onto titanium relevant for guiding osteogenic differentiation of MSCs.

To achieve the goal of the study, the main objectives had to be determined. Firstly, the desired patterns have to be designed. These patterns are obtained from literature research. Secondly, the main process steps need to be determined. Thirdly, the process conditions have to be determined for the pattern writing and the pattern transfer into titanium.

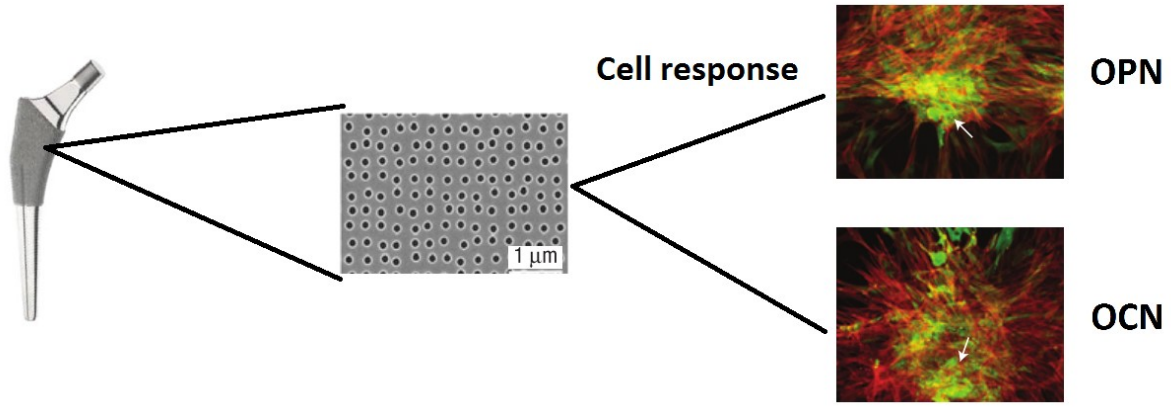

Figure 1: A non-cemented stem of a hip implant, with the optimal nanotopography that is created by Dalby et al. [12] on a PMMA substrate. The cell response on this topography can also be seen. The cell response is expressed in levels of osteopontin (OPN) and osteocalcin (OCN). OPN and OCN are components of the extracellular matrix and are markers for osteogenic differentiation.

2 Materials and Methods

In this chapter the methods to create the patterns into titanium are described. Firstly, the substrate is described (section 2.1), with two sections, one on commercially pure titanium (section 2.1.1), and one on evaporated film titanium (section 2.1.2). Secondly, the patterning is described (section 2.2), with the design (section 2.2.1), the EBL process steps including the resist (section 2.2.2), and the pattern writing and dose test (section 2.2.3). Thirdly, the pattern transfer into the titanium is described (section 2.3). Fourthly, scanning electron microscope (SEM) inspection methods are described (section 2.4).

2.1 Substrate

To pattern titanium, a titanium substrate is needed. Two different substrates have been considered: commercially pure titanium (section 2.1.1), and a thin titanium film on a flat substrate (section 2.1.2).

2.1.1 Commercially Pure Titanium

The clinical application of the patterns into titanium is the joint replacing implant. In order to move towards this clinical application commercially pure titanium should be used as a substrate. Titanium discs, of 8 mm in diameter, were ordered. However, the titanium discs, as ordered have a high surface roughness. To be able to pattern a submicron/nanotopography onto the surface, it was needed to create a smooth surface finish. Therefore, polishing was applied to smoothen the surface of the titanium discs.

Before polishing the discs were grinded to prepare the surface for polishing. Both grinding and polishing were performed manually and automatically. Both procedures used a slightly different approach and were both based on the process of Sittig et al. [23].

The manual grinding procedure, made use of several different sizes of grinding paper. The sizes of grinding paper used were 320, 800, 1000, 2000, and 4000. After each step, the disc was inspected by optical microscopy, to determine if the grinding step has been sufficient. In between each of the grinding steps, the discs were cleaned inside an ultrasonic bath with ethanol, to remove any particles or debris left from the previous grinding step. After grinding, polishing was performed. There was only one polishing step, this was polishing with an OP-S solution.

During automatic grinding and polishing, there were several machine variables to control. The machine used for automatic polishing is the Struer RotoForce-4. The machine variables were set to a pressure of 10 kN, a clockwise specimen rotation of 300 rpm, with a force reduction towards the end of the cycle. There were four steps taken during automatic grinding and polishing. Firstly, a step with grinding paper size 800 for 1:30 min. Secondly, a step with grinding paper size 1200 for 2 min. Thirdly, the last grinding step with grinding paper size 2400 for 30 s. Fourthly, a polishing step was applied with OP-S. In between all the steps the specimen was inspected by optical microscopy, to determine if the previous step has been sufficient. Also, the specimen was rinsed thoroughly with tap water, in between each step, to clean the specimen from any particles, and debris left from the previous step.

After polishing, surface roughness measurements were performed. The surface roughness was measured on the DektakXT. This device runs a tip over the surface and measures the height deviation. This deviation is displayed into a height-length graph.

2.1.2 Evaporated Titanium Film

To pattern micro/nanotopography onto titanium, a flat substrate is needed. To obtain this perfectly flat substrate of titanium, a titanium film was used. This titanium film was deposited onto a 4-inch silicon wafer, by evaporation.

In evaporation the substrate is placed, upside down, into a vacuum chamber. This chamber is pumped down until vacuum. When the system is under vacuum, an electron beam is used to heat the evaporation source [24]. The evaporation source is located on the bottom of the vacuum chamber. When the source is heated and the metal is evaporating at the subscribed rate, the shutter is opened, and the formation of the thin film starts. The resulting layer is evenly distributed along the surface of the substrate.

During this experiment the TEMESCAL FC-2000 equipment was used to create the titanium substrate (see Figure 2). Titanium (99.5 % pure) was used evaporation source. A layer of 200 nm titanium was evaporated on top of the silicon wafer. The evaporation rate used was 2 Å/s, and the process starting pressure was $3 \cdot 10^{-6}$ Torr. The evaporation process gave the smooth surface required for patterning.

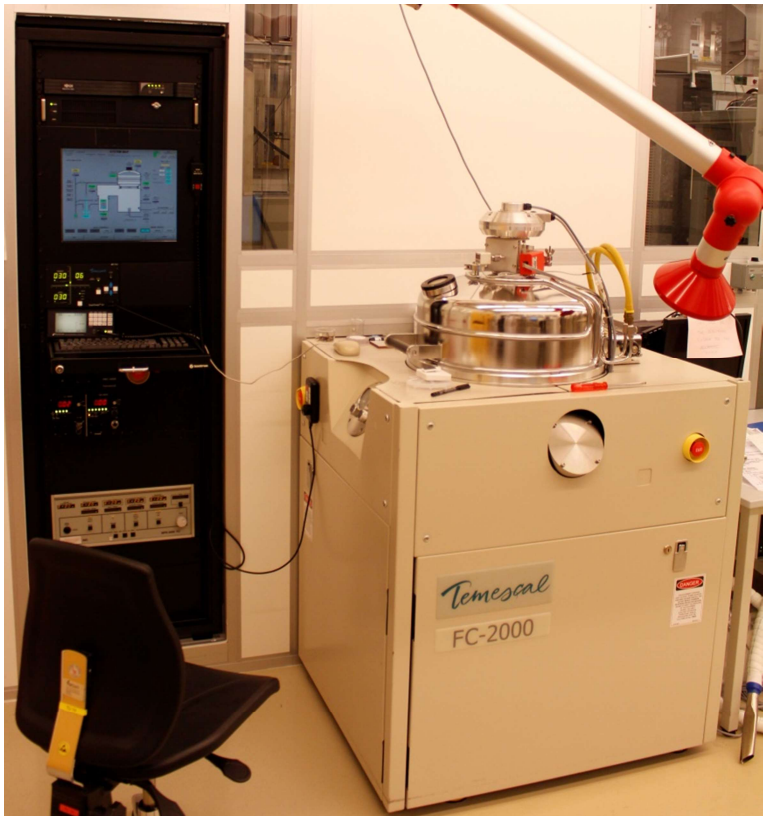

Figure 2: Evaporation equipment, used to evaporate titanium on to a 4-inch silicon wafer (Temescal FC-2000). On the right, the evaporator is seen , with the load lock (dome). On the left the control unit is seen.

2.2 Patterning

During patterning the designed pattern is written into a layer of resist. The patterning is performed by EBL, due to the small features of the pattern. Firstly, the design of the pattern is described (section 2.2.1). Secondly, the EBL process steps and the resists are described (section 2.2.2). Thirdly, the pattern writing and the dose test are described (section 2.2.3).

2.2.1 Pattern Design

The design of the patterns was determined by literature research. It was needed to design a series of patterns that includes patterns of the most promising studies, on osteogenic differentiation. From literature, one article was very promising towards osteogenic differentiation, the article of the group of Dalby [12], performed on PMMA. In this research differentiation of MSCs into osteoblasts, is achieved without the use of osteogenic media. Furthermore, this group performed research onto different patterns, to determine the optimal

pattern to induce osteogenic differentiation [13], also on PMMA. This group uses circular features, hence circular features were also chosen for this study.

Based on literature, several variables were identified for the pattern series. These were the: pattern diameter, pattern depth/height, and pattern disorder. Disorder is a set distance of the feature from the square position, in a random direction. The missing variable is the interspacing. The interspacing is the distance between the centres of the individual dots. Hence, the interspacing was also included in the designed series of patterns. Selected pattern variables are as follows (some typical examples can be seen in Figure 4):

- Diameter: 30 nm, 50 nm, 100 nm, 200 nm, 300 nm, 500 nm.
- Disorder: 0 nm, 15 nm, 30 nm, 50 nm, 75 nm.
- Interspace: 300 nm, 900 nm.

To incorporate the disorder, a MATLAB program was written to determine the dot position (see Appendix A – Controlled disorder). This MATLAB program was based on the disorder and interspacing to determine a particle coordinate. These coordinates were determined for a 10x10 square array, after which this array was repeated to create the required area. All chosen patterns can be seen in Appendix B – Patterns.

The pattern design was created in L-Edit, which is a program that is suited for the design of microelectronics. Basic shapes such as the dots, that are in the program, are easily created into the design. The position of each circle can be put in by hand, however it is also possible to create an array in square arrangement. The design from L-Edit can be seen in Figure 3, where one pattern is enlarged.

The design was exported to a GDSII format, to upload onto the EBL surfer. From the GDSII file a job file was created. This job file was read by the machine and patterned onto the substrate.

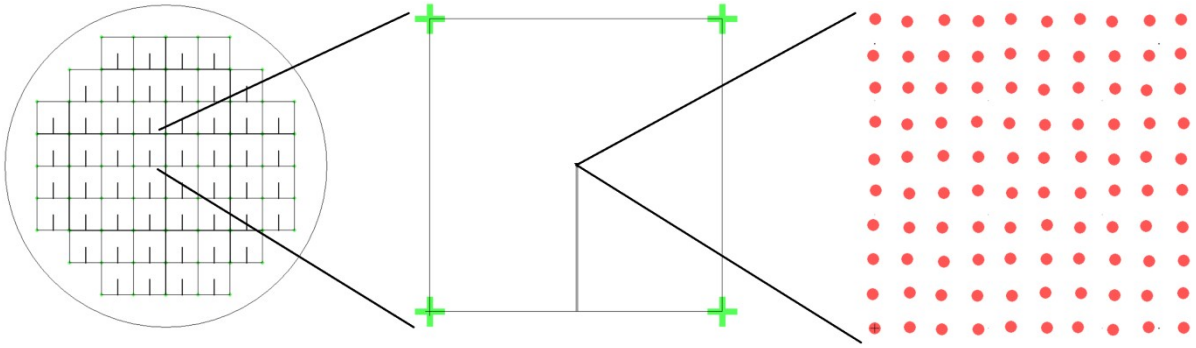

Figure 3: The design of the total wafer. One pattern is enlarged from this design. This is the pattern with 100 nm diameter, 300 nm interspacing, and 15 nm disorder. The characteristics of all patterns can be seen in Appendix B – Patterns.

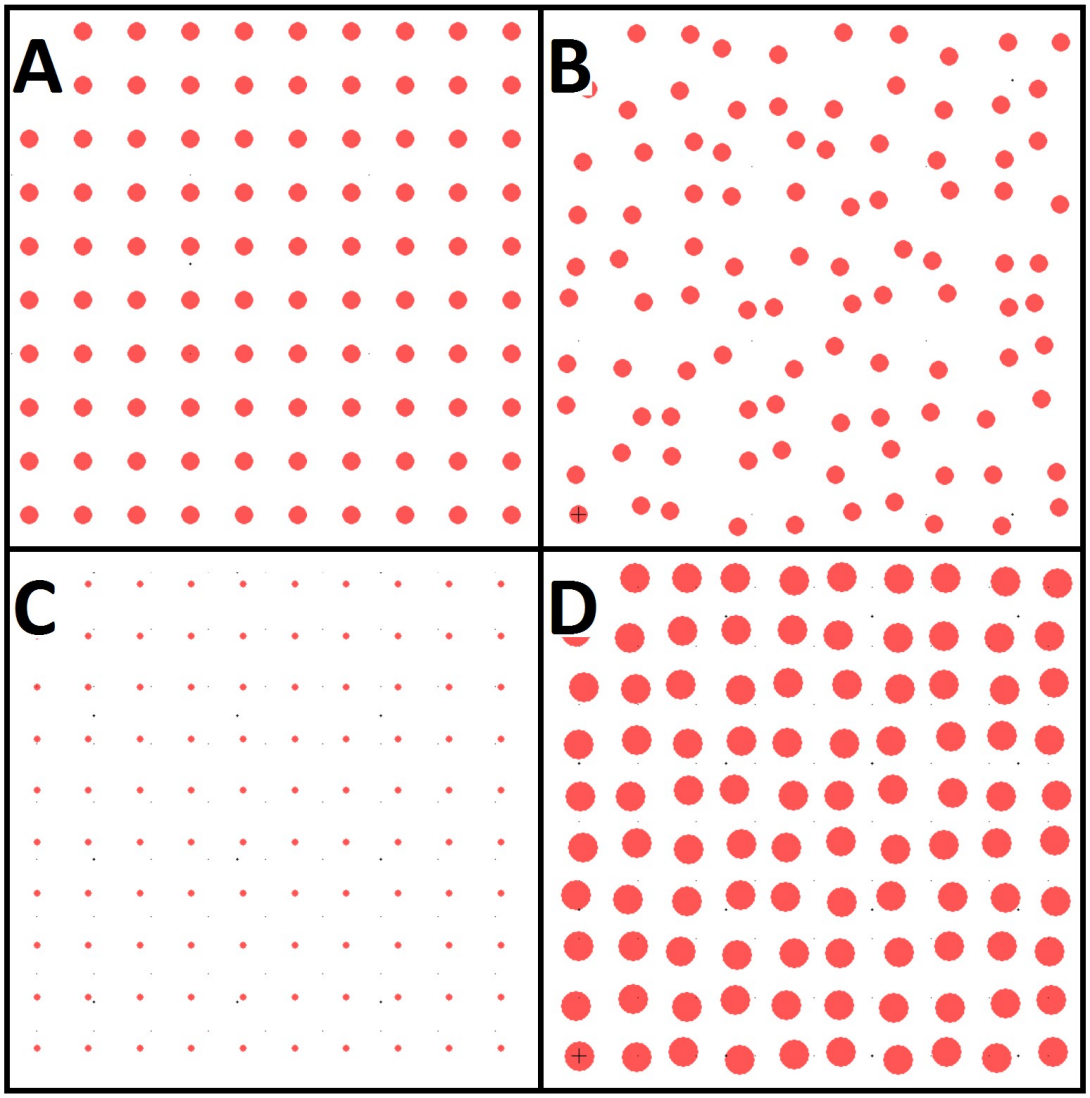

Figure 4: Some typical patterns used in the design. A) 100 nm dots, in square arrangement, with an interspacing of 300 nm; B) 100 nm dots, with a controlled disorder of 75 nm, with an interspacing of 300 nm; C) 100 nm dots, in square arrangement, with an interspacing of 900 nm; D) 500nm dots, with a controlled disorder of 75 nm, with an interspacing of 900 nm.

2.2.2 Electron Beam Lithography Process Steps

During EBL there are several steps included. These steps can be seen in Figure 5. The process starts with a silicon wafer, onto which 200 nm titanium is evaporated. After the evaporation a distinction is made between the resist mask and the hard mask. The resist mask procedure follows the black arrows in Figure 5, and the hard mask procedure follows the green arrows in Figure 5.

For the resist mask, the resist is applied onto the evaporated titanium. After the resist is applied the EBL process can start. A description of this process is given in section 2.2.2.1. For the hard mask, the hard mask itself needs to be applied. After the application of the hard mask the resist is applied. A description for this process is given in section 2.2.2.2. After writing, the pattern is developed. This process is the same for both the resist mask and the hard mask (section 2.2.2.1). When the resist is developed, the pattern is transferred into the titanium (see section 2.3).

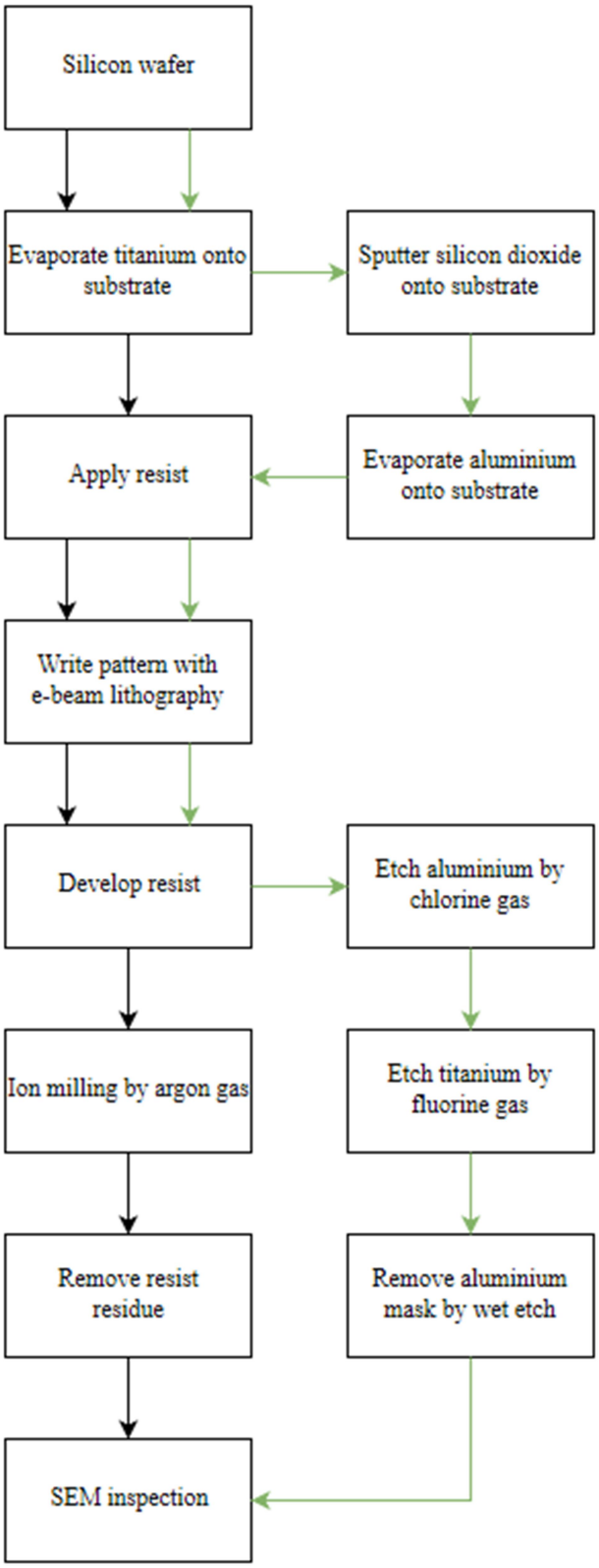

Figure 5: Flowchart for the two designed processes. The black arrows indicate the process used with only the resist as an etching mask. The green arrows indicate the process used with the hard mask.

2.2.2.1 Resist mask

As mentioned above, the resist was patterned by EBL. The resist is a mixture of polymers in liquid form. These polymers are evenly distributed onto the surface, by using a spinning table. When this even liquid layer of resist is applied, the resist is cured on a hotplate or in an oven.

There are two types of resist, negative resist and positive resist. The positive resist consists of cross-linked polymers. When this positive resist is bombarded by electrons, like in EBL, the polymers are fragmented and become more soluble into the developer liquid. The negative resist consists out of fragmented polymer chains. When this negative resist is bombarded by electrons, the polymers are cross-linked and become less soluble in the developer liquid. The difference between the negative and positive resist, after development, is seen in Figure 6.

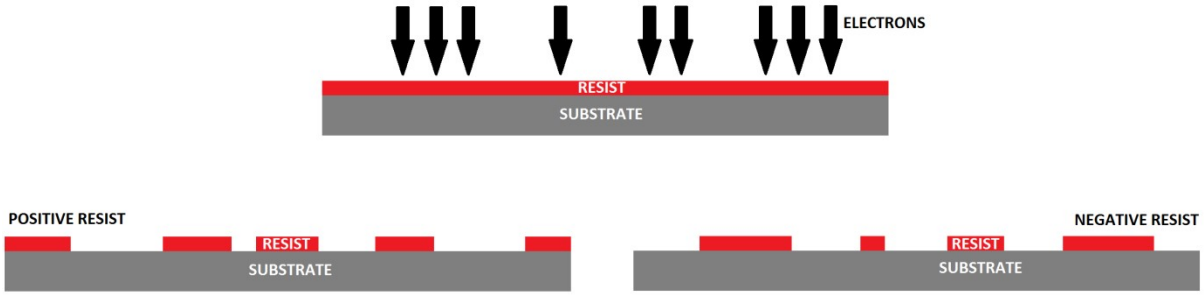

Figure 6: The difference between positive resist (left) and negative resist (right) after writing and development.

To pattern the small features by EBL a suitable resist was chosen. Both chosen resists are obtained from the company All Resist. The positive resist chosen is AR P-6200.04. The P-6200 series has the required resolution, and the .04 has the possibility to lower the layer thickness to 100 nm. The negative resist chosen is AR N-7500.08. The N-7500 series leads to the required resolution, and the .08 leads to the required layer thickness of 100 nm.

The application of the resist was performed by a spinning table, and a hotplate. For the positive resist, a rotation speed of 3500 rpm was used to achieve a layer thickness of 100 nm. After spinning the resist was baked for 3 min on a hotplate at 150 ˚C. The negative resist needed a primer before the resist was applied. The primer used was Hexamethyldisilazane (HMDS), this needed to spin at 2000 rpm, and bake for 2 min on a 200 ˚C hotplate. On top of the HMDS the resist layer was applied. The layer thickness of 100 nm was achieved with a rotation speed of 4000 rpm. After application, the resist was baked for 1 min on a hotplate at 85 ˚C. After application of both resists, the substrates were ready for EBL, which is described in section 2.2.3.

After EBL (the electron bombardment of the resist), the resist needs to be developed in order to reveal the patterns. The development is performed by chemicals that dissolve the non-crosslinked parts of the resist. For the positive resist, the development procedure used was: 60 s in amyl acetate, followed by 60 s in a 1:1 solution of methyl isobutyl ketone : isopropyl alcohol, and 60 s in isopropyl alcohol. The negative resist, is developed for 60 s in MF322 developer, and rinsed with water.

When this pattern is transferred into the substrate, the resist needs to be removed. The removal of the resist is performed by using oxygen plasma. The system used for this removal was the Tepla stripper 100. The settings used were 200 mL/min oxygen flow, a power of 600 W for 10 min duration, without the faraday cage.

After the application of the resist, the substrate preparation is finished. The substrate consists of the silicon wafer, with an evaporated layer of titanium of 200 nm, onto which the resist layer of 100 nm is applied. In Figure 7 the configuration of this wafer can be seen.

Figure 7: Configuration of the substrate, with a resist applied before patterning. On the bottom the silicon wafer, on top of the wafer 200 nm evaporated titanium and on top the resist.

2.2.2.2 Hard Mask

During reactive ion etching (RIE) (section 2.3), it became apparent that a resist mask is not sufficient to etch titanium. The resist mask was removed before any pattern was transferred into the titanium. To solve this problem a hard mask solution was obtained from literature [25]. The mask described by Löffler et al. was adjusted to suit the feature size in this study. The layer of silicon dioxide was lowered from 20 nm to 8 nm, and the layer of aluminium was lowered from 100 nm to 40 nm. Aluminium was used as an etching mask, because of the favourable properties in fluorine gas. Aluminium did not react with the fluorine ions.

When the hard mask is applied there is still a resist needed. This resist is needed for EBL. Like in the resist mask both the same positive and negative resist are used. For the application and the development of the resist, the same procedure as for the resist mask is used (described in section 2.2.2.1).

After the application of the resist, the substrate preparation is finished. The substrate is composed of the silicon wafer, with 200 nm evaporated titanium on top of the wafer. On top of the titanium the 8 nm silicon dioxide layer is applied, after which the 40 nm aluminium hard mask is applied. This is the hard mask. The resist layer of 100 nm is applied on top of the hard mask. In Figure 8 the configuration of the wafer can be seen.

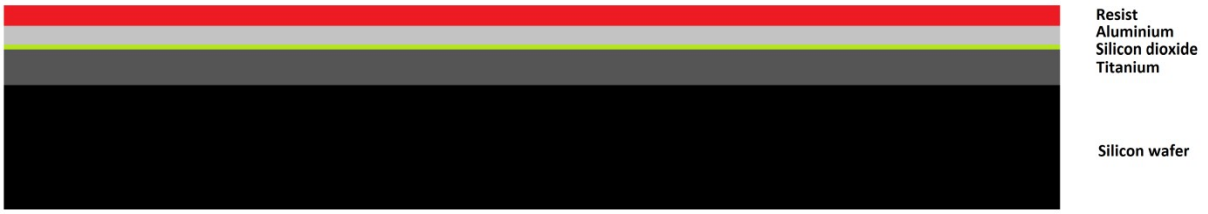

Figure 8: Configuration of the hard mask solution, with resist applied before patterning. On the bottom the silicon wafer, on top of the wafer the 200 nm evaporated titanium, on top of the titanium 8 nm silicon dioxide, on top of the silicon dioxide 40 nm aluminium and on the top the resist layer.

2.2.3 Pattern Writing & Dose Test

As mentioned in the previous section, EBL is used to pattern the resist. The bonds in the resist are either broken, or formed when the electron beam is directed onto the resist. The electrons travel from the source, the cathode, towards the substrate, through a set of optical elements. These optical elements focus and control the electron beam, and are located inside the column. The optical elements inside the column are (from top to bottom): the source that consists out of a field emission gun, magnetic lenses for pre-focussing, beam alignment with an aperture to correct shift and tilt of the beam, more magnetic lenses for focussing, the blanker to interrupt the beam when necessary, beam positioning by another aperture, again magnetic lenses to fast focus and tune the beam [26]. The substrate is positioned on the

bottom of the electron column, and is mounted on a stage which, can move in the horizontal field.

During EBL, writing is performed in spots. The substrate is divided into writing fields. There are two types of writing fields. The first type is the main field in which the stage has to make a horizontal movement in order to put the beam in that field. The second field (beam deflected field) is inside the main field, these are the fields to which the beam is deflected to write onto a certain spot. The beam step size (BSS), is the magnitude of this beam deflection, inside the beam deflected field. With this BSS, the beam spot size (d_{spot}) can be calculated by equation 2.1 [27]. It is important, in order to ensure quality, that at least 4-5 spots are located within one linewidth.

$$d_{spot} = 1.2 - 1.5 \cdot BSS \qquad \text{Eq. 2.1}$$

The machine uses a vector scan to write onto each field. During a vector scan, all features are divided into trapezoids. The trapezoids are written from the left bottom, towards the top, in a serpentine order.

The number of electrons that are deposited onto the substrate by the electron beam are given in $\mu C/cm^2$, the dose. This dose is different, for each type of resist and substrate combination. The dose is a function of the current, the frequency, and the BSS. The function for the dose is seen in equation 2.2 [27].

$$Dose = \frac{Current}{Frequency \cdot BSS^2} \qquad \text{Eq. 2.2}$$

The correct dose is essential for the pattern. With a dose that is too low, the pattern will be too small or even missing after development. With a too high dose the pattern will be too large after development. To obtain the correct dose, a dose test needed to be performed. With the use of this, experimentally determined, correct dose, the pattern is written into both resists.

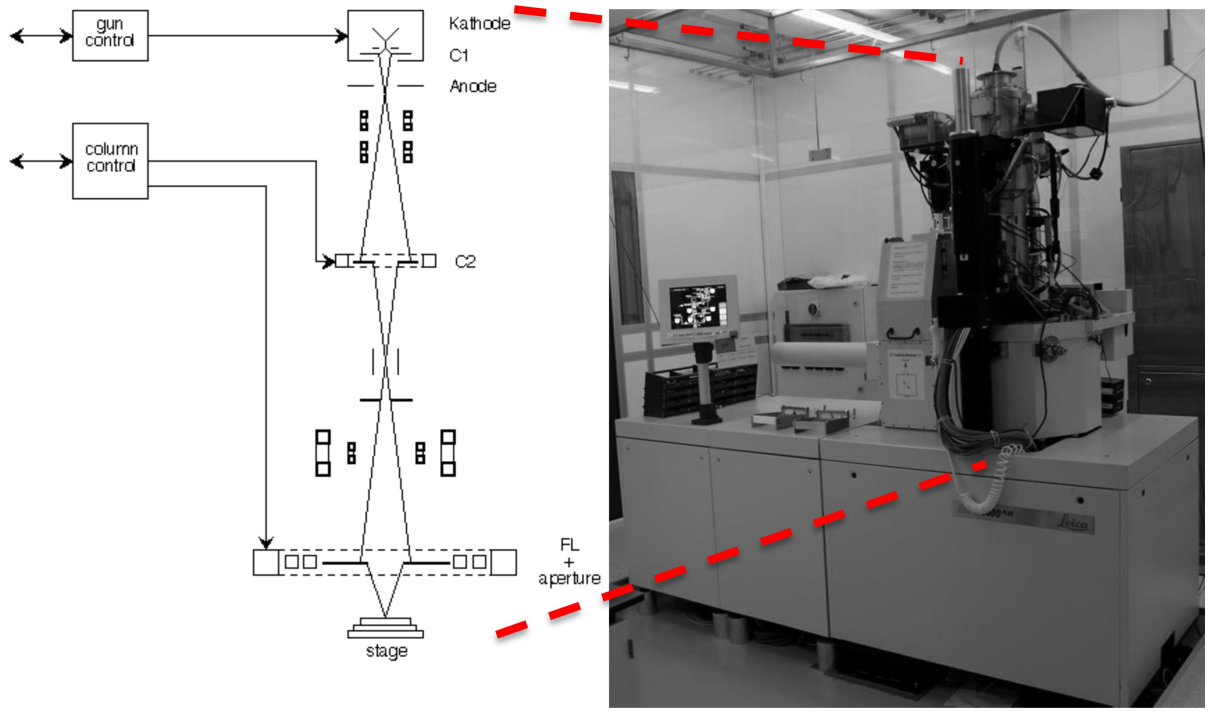

Figure 9: The EBL equipment. On the left a schematic of the electron column [27], with the source and the optical elements. On the right the EBL equipment is seen, in which the electron column is indicated.

As mentioned above, a dose test is needed for each resist and substrate combination, to determine the optimal dose. This dose changes for each resist and substrate combination, due to electron scattering. This electron scattering consists out of forward scattering and backscattering.

Forward scattering (α) is the phenomenon in which the electrons interact with other electrons that they encounter inside the resist. This forward scattering leads to beam broadening of about 1-10 nm. The range in which forward scattering occurs is dependent on the resist material, the resist thickness, and the acceleration voltage used.

Backscattering (β) occurs due to the electrons that travel further than the resist, into the substrate. These electrons scatter in all directions upon contact with the substrate, also back towards the resist. This contributes to the exposure of the resist, in a range of ~10 μm. The backscattering is dependent on the substrate material, and the acceleration voltage used.

The scattering effects can be approximated by a model. However, to know exactly what the effects are and what the best dose is, an experimental dose test is still needed. The approximation of the scattering effects (PSF) is given in equation 2.3 [27], where η is the ratio of the backscattered energy to the forward scattered energy.

$$PSF(r) = \frac{1}{\pi(1+\eta)}\left[\frac{1}{\alpha^2}e^{-\left(\frac{r^2}{\alpha^2}\right)} + \frac{\eta}{\beta^2}e^{-\left(\frac{r^2}{\beta^2}\right)}\right] \qquad \text{Eq. 2.3}$$

To perform the dose test, a design is needed. A pattern that is similar to the chosen pattern is designed, to take the electron scattering into account. The pattern used for the dose test consists out of the smallest and the largest feature used, at the smallest interspace distance. Also, a marker is added to be able to find the small structures during inspection. The chosen patterns for the resist mask were dots of 50 nm and 200 nm in diameter. The chosen patterns for the hard mask dose test, are slightly different, and can be seen in Appendix C – Dose Test Design. The diameter was chosen to be 100 nm for the small feature, and 500 nm for the large features. This different feature size for the hard mask dose test, was chosen after imaging the results during the pattern transfer.

The total dose test was performed four times. Once for: the positive resist on the titanium surface, the negative resist on the titanium surface, the positive resist on the hard mask, and the negative resist on the hard mask. After the dose tests, the resist was developed and subjected to SEM inspection (section 2.4). Both the positive, and the negative resist have prescribed doses, from the manufacturer, these are ~250 μC/cm^2 for the positive resist, and ~1600-1700 μC/cm^2 for the negative resist. Therefore, for the positive resist, the dose test started at 200 μC/cm^2, and was increased by a factor of 1.2 for every dose update, there were 9 dose updates. For the negative resist, the dose test started at 1500 μC/cm^2, and was increased by a factor of 1.2 for every dose update on the resist mask on top of the titanium, with 9 dose updates. The increase for the hard mask configuration was a factor of 1.1 for each dose update, with 9 dose updates. The different doses used during the dose test can be seen in Table 2.

During SEM inspection the resist pillars and pits are measured. The optimal dose was determined by measuring the resist pit and pillar size, and comparing them to the specified dimensions. Also, it is important with positive resist to check if the holes are completely open. From the inspection the best pattern of the resist was determined and chosen for the patterning of all the structures.

Table 2: The doses used during the four dose test. For both the resist mask and the hard mask, and also for both the positive and the negative resist.

Resist mask		Hard mask	
Positive resist dose [μC/cm^2]	**Negative resist dose [μC/cm^2]**	**Positive resist dose [μC/cm^2]**	**Negative resist dose [μC/cm^2]**
200	1500	200	1500
240	1800	240	1650
288	2160	288	1815
346	2592	346	1997
415	3110	415	2196
498	3732	498	2416
597	4479	597	2657
717	5375	717	2923
860	6450	860	3215
1032	7740	1032	3537

2.3 Pattern Transfer

By EBL and the development, the pattern is only transferred into the resist. In this research there were two different etching methods used to transfer the patterns into the titanium, both with different results. The first one was reactive ion etching (RIE) and the second one was ion milling. Both methods for the pattern transfer can also be seen in Figure 5, the process flowchart.

In RIE the substrate is placed into a vacuum chamber. The substrate is positioned on top of the electrode that is connected to the radio frequency (RF) power source. The top of the chamber is the other electrode that is connected to the ground. When vacuum is achieved, the etching gas is let into the chamber with a constant flow rate. The gas flow is ignited by the RF power source to form a plasma between the two electrodes. The ions formed in this plasma are accelerated towards the substrate, and react with the substrate. Material from the substrate is desorbed into the gas mixture, and removed via the gas outlet leading to the removal of the layers on the substrate, and hence etching the material. [28]

There are several different gases present to use for etching. Inside the fluorine RIE machines (Leybold Hereaus, as seen in Figure 10), there are fluorine based gases present, oxygen, helium, and argon. Inside the chlorine RIE machine, there are chlorine based gases present, oxygen, argon, helium, bromine, and nitrogen. With these gases all different combinations, within one machine, can be made, to find a recipe to etch the titanium.

Ion milling, is approximately the same process as RIE. However, there are no reactive ions included in the process. The gas that was inserted into the chamber was argon. With the argon gas the plasma was formed by a RF power source. However, now the ions are used to bombard the surface of the substrate. Due to this bombardment, the titanium is etched away. Another difference is that the bombarded ions do not dissolve into the gas. They are deposited elsewhere on the structure. This can be on the resist, which is removed later, or somewhere else on the structure. The machine used for ion milling is the Alliance concept Ac450 (Figure 11).

Figure 10: RIE equipment used (Leybold Hereaus). On the right the control system can be seen, and on the left the chamber (cylindrical) can be seen.

Figure 11: Ion milling equipment used (Alliance concept Ac450). On the front the load lock of the machine can be seen.

The recipes for titanium etching were obtained from both literature, and other user experience. The recipes in literature are difficult to convert to the RIE machine that is inside the Kavli laboratory. This difficulty arises from the fact that all machines are slightly different, so every recipe has to be changed slightly.

A schematic of both etching process can be seen in Figure 12. In this schematic the difference between the positive and negative resist can be seen during etching. In the bottom images the remaining resist is also stripped by oxygen plasma.

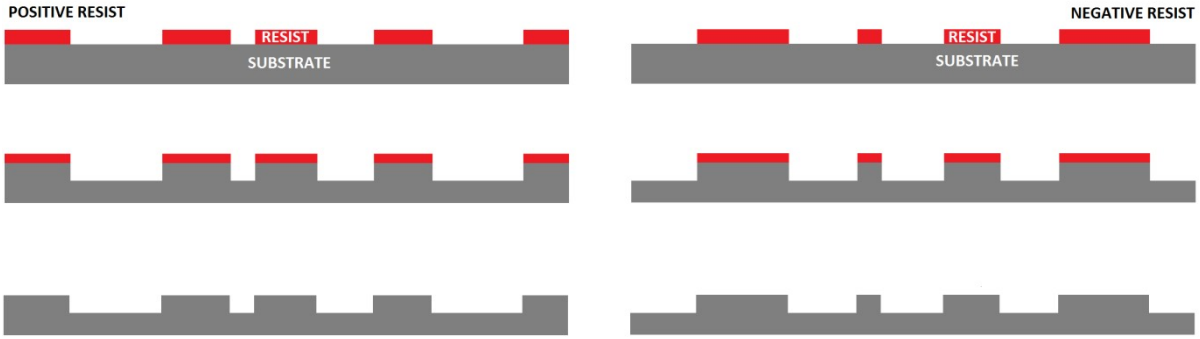

Figure 12: A schematic of the etching process for the negative and the positive resist. The top image is the substrate with the pattern after EBL and development. The second image is the substrate after the etching process. The third image is the substrate after the removal of the resist mask.

There were several different recipes tried to etch titanium. Both fluorine and chlorine gases were tried. The recipes tried, as seen in Table 3, were obtained either from literature, or from other user experience. For process 8 and 9 there is no power used described. This is because the power on this machine was not accurate, and the bias voltage was used as a reference. Also another recipe was found in literature [29], using CF_4 and Cl_2. However, this was not applicable inside the Kavli laboratory. Inside the Kavli laboratory it is not possible to combine CF_4 and Cl_2 within one machine. In Table 4 the overview for the recipes and the mask on which they are used is seen.

The etching procedure for the hard mask, started with an etch through the aluminium. To etch through the aluminium, a standard chlorine dry etch for aluminium, developed by other users, was used. This process has 4 steps: temporization, breakthrough, Al etch, and pump-out. During the temporization process, no gases are present in the chamber, and the chamber temperature is elevated to 50 ˚C for the process. The breakthrough step (Recipe no. 13 in Table 3) is to break through the surface layer of aluminium oxide. During this process a plasma is formed consisting out of BCl_3 (30 sccm) and Cl_2 (5 sccm) for 25 s, with a power of 200 W. During the Al etch step (Recipe no. 14 in Table 3), the same gas composition as in the breakthrough step was used, however the power was lowered to 100 W, and the process duration was 30 s. The pump-out step is to pump all the remaining gases from the chamber. After the dry etch of aluminium, the substrate was put into the RIE machine to etch the titanium by fluorine gas, with the same composition as used by Löffler et al. [25], also seen in Table 3, as recipe number 11.

However, this layer of aluminium, the hard mask, on top of the titanium cannot be removed with oxygen plasma after etching. The removal procedure of the hard mask is performed by a chemical aluminium wet etch [30]. Aluminium etch type D (recipe number 15) was used. It was needed to etch for 7:30 min before the layer of 40 nm was removed.

Table 3: Different gas compositions used during the RIE and ion milling procedure

Recipe No.	Gases [sccm]			Power [W]	Bias [V]	Time [s]	Ref.
1	50 Cl_2	2.5 Ar		1000	-90	15	[31,32]
2	50 Cl_2			1000	-90	15	[31,32]
3	100 CF_4			43	-528	60, 120, 180	Experience
4	100 CF_4	1 O_2		42	-517	60, 120, 180	Experience
5	95 CF_4	5 O_2		42	-500	60, 300	Experience
6	98 CF_4	2 O_2		40	-435	60	Experience
7	20 CF_4	50 Ar		32	-469	300, 600	[33]
8	100 SF_6	0.6 O_2			-249	300	Experience
9	100 SF_6	1.2 O_2			-258	300	Experience
10	25 CHF_3	25 Ar		37	-530	90	Silicon recipe
11	13 SF_6	13 CHF_3	15 O_2	100	-280	180	[25]
12	30 Ar			100	-675	150, 300	Experience
13	30 BCl_3	5 Cl_2		200		25	Experience
14	30 BCl_3	5 Cl_2		100		30	Experience
15	Aluminium wet etch type D			-	-	450	[30]

Table 4: Overview of the processes used on the different substrate configurations.

Process		Resist mask		Hard mask	
Name	**Recipe No.**	**Positive resist**	**Negative resist**	**Positive resist**	**Negative resist**
RIE	1	-	+	-	-
RIE	2	+	+	-	-
RIE	3	+	+	-	-
RIE	4	+	+	-	-
RIE	5	+	+	-	-
RIE	6	+	+	-	-
RIE	7	+	+	-	-
RIE	8	+	+	-	-
RIE	9	+	+	-	-
RIE	10	+	-	-	-
RIE	11	+	+	+	+
Ion milling	12	-	+	-	-
Al etch	13	-	-	+	+
Al etch	14	-	-	+	+
Al wet etch	15	-	-	+	+

After etching there can be 2 results: anisotropic etching and isotropic etching. For isotropic etching, the etch rate is the same in all directions. For anisotropic etching, the etch direction is only downwards. Both principles can be seen in Figure 13. During etching it is preferred to have anisotropic etching, such that the etched features resemble the mask. Anisotropic etching is often accomplished by the correct RIE conditions, isotropic etching is always accomplished by a wet etch, or is accomplished by the wrong gas composition during RIE.

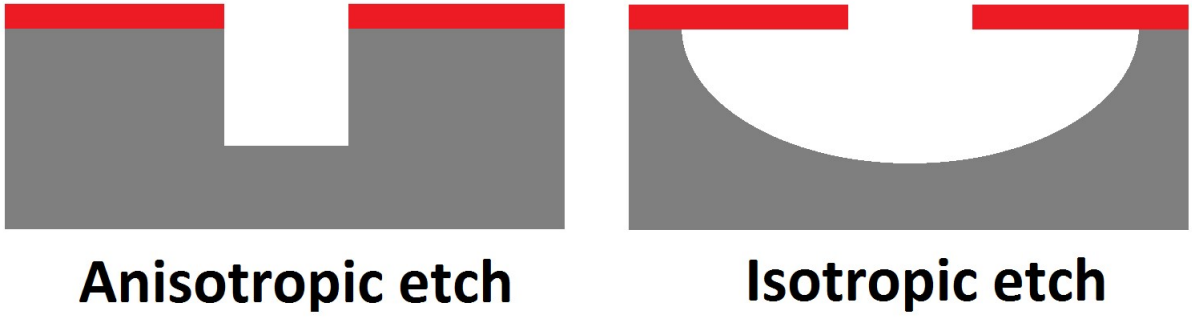

Figure 13: The difference between an anisotropic etch, and an isotropic etch.

2.4 Scanning Electron Microscope (SEM) Inspection

After the dose tests and etching, inspection was performed to image the results. This inspection was performed by a SEM (seen in Figure 14). A SEM has an electron gun, that shoots electrons towards the substrate. The electrons are guided through a set of magnetic lenses and an aperture, to focus the beam. To obtain an image the secondary electrons emitted from the substrate are translated into the image. With these secondary electrons, the substrate topography can be imaged.

There are two main variables during SEM imaging: the accelerating voltage, and the emission current. An increase of the accelerating voltage leads to a decrease in lens aberrations and a higher resolution, an increase in the probe current with potentially charge-up in the non-conductive specimen, and an increase of beam penetration into the specimen which can obscure surface details. An increase in the beam current leads to an increase of the current at the specimen, which potentially increases the charge-up and damage in the non-conductive specimen.

This means that a low acceleration voltage, 5kV, was used to image the resist during the inspection of the dose test, to have minimal charge on the non-conductive resist substrate. For imaging the titanium structures, an accelerating voltage of 15kV was used, to obtain a sharp image.

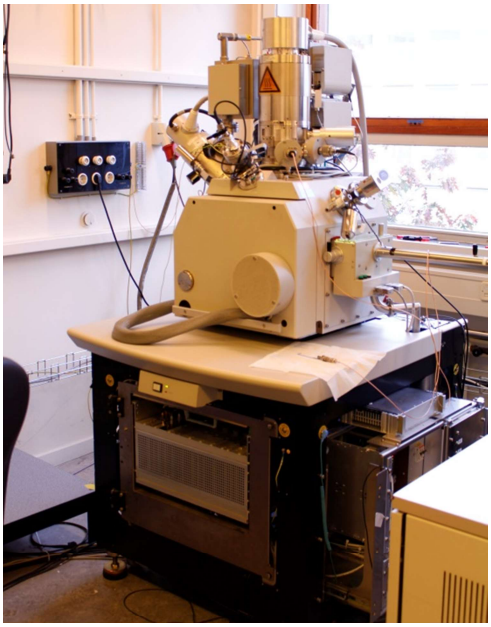

Figure 14: SEM equipment, used for inspection of the results.

3 Results

In this chapter the results of the conducted study are given. Firstly, the substrate characterisation results are given on polishing (section 3.1). Secondly, the results on patterning are given, from the dose test (section 3.2) for both the resist mask (section 3.2.1), and the hard mask (section 3.2.2). Thirdly, the results on the pattern transfer are given (section 3.3), where both the results on the RIE procedure (section 3.3.1), and the ion milling (section 3.3.2) are given.

3.1 Substrate Characterisation

In this section the results for polishing are given. During this study two types of substrate were considered: commercially pure titanium discs and evaporated film titanium. Both substrates were imaged by SEM before any procedure was performed on the substrate. The results can be seen in Figure 15. In Figure 15A the commercially pure titanium discs as ordered can be seen. From this SEM image, large grains, some voids, and the micro roughness can be seen. The roughness was measured, and calculated to have a value of Ra = 352 nm. In Figure 15B the evaporated film titanium can be seen, here the grains are very small and there is almost no roughness visible. On this substrate the roughness was measured to be Ra = 3.8 nm.

As mentioned in the materials and methods (section 2.1.1), the established polishing procedure was carried out on the titanium discs. The resulting substrate surface for automatically polishing can be seen in Figure 16. The roughness of al substrates was measured with the DektakXT. For manual polishing the roughness that could be obtained was Ra = 61.5 nm. For automatic polishing the roughness obtained was Ra = 28.6 nm. The measurement data is included in Appendix D – Roughness measurements.

From the obtained roughness data and inspection, evaporated titanium was chosen as a substrate. The manually polished titanium discs were discarded due to the roughness. Some of the intended patterns are smaller than the roughness, hence it would be difficult to distinguish the pattern from the surface roughness. The automatic polished commercially pure titanium discs a better roughness was obtained. It would be possible to pattern onto this surface. However, the automatically polished discs were discarded due to the voids inside the material. The voids were large, compared to the pattern size. These voids can lead to a loss or a partial loss of the pattern, when the pattern is placed on such a void. Hence, the substrate used during this study was determined to be an evaporated titanium film onto a 4-inch silicon wafer.

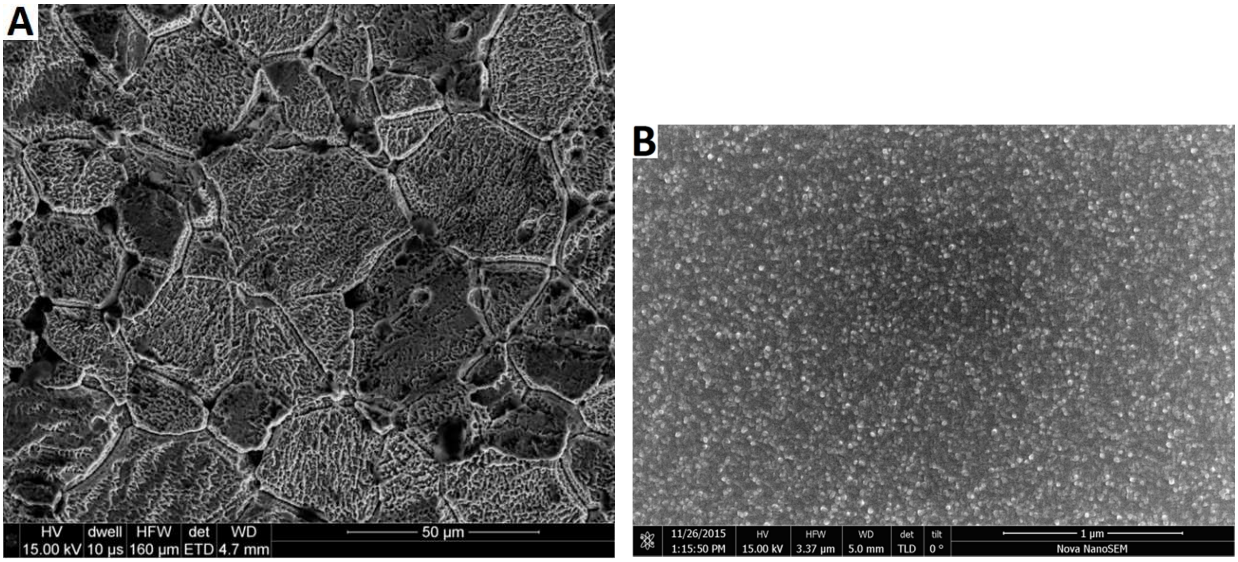

Figure 15: A) SEM image of the commercially pure titanium discs that as ordered. The micro surface, grain structure, and the micro roughness can be seen. B) SEM image of the evaporated titanium, the grain size is small and the surface is smooth.

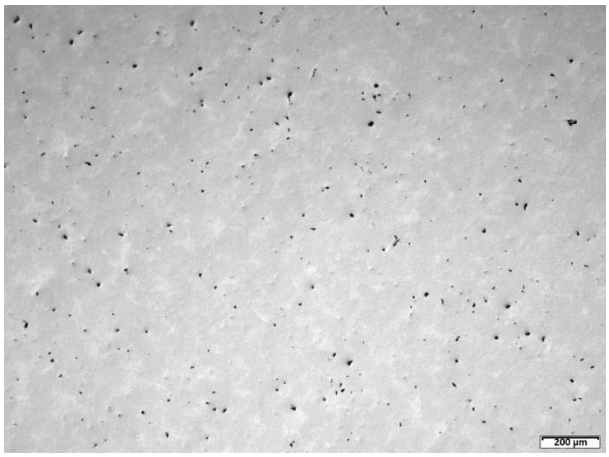

Figure 16: Optical microscope image of the result of automatic polishing, the scale bar is 200 µm. The surface texture can be seen, some voids in the material and some micro roughness can be seen on the surface.

3.2 Patterning

Patterning of the substrate was performed by EBL. To pattern the design, the dose required needs to be determined. The results of the dose test are given in this section. Both the dose test of the resist mask (section 3.2.1), and the dose test of the hard mask (section 3.2.2) are given.

3.2.1 Dose Test For The Resist Mask Process

The dose test results for the resist mask are described in this section. From SEM inspection, the resist topography was studied for both the positive, and the negative resist. For the positive resist (pits) it was determined that a dose of 346 µC/cm^2 is optimal. This is dose number 4. The SEM result, for this dose, can be seen in Figure 17. In Appendix E – Dose Test Images Figure 39, and Figure 40 images are seen for the lowest and the highest dose. The effect of the different doses on the pattern diameter can be seen in Figure 18.

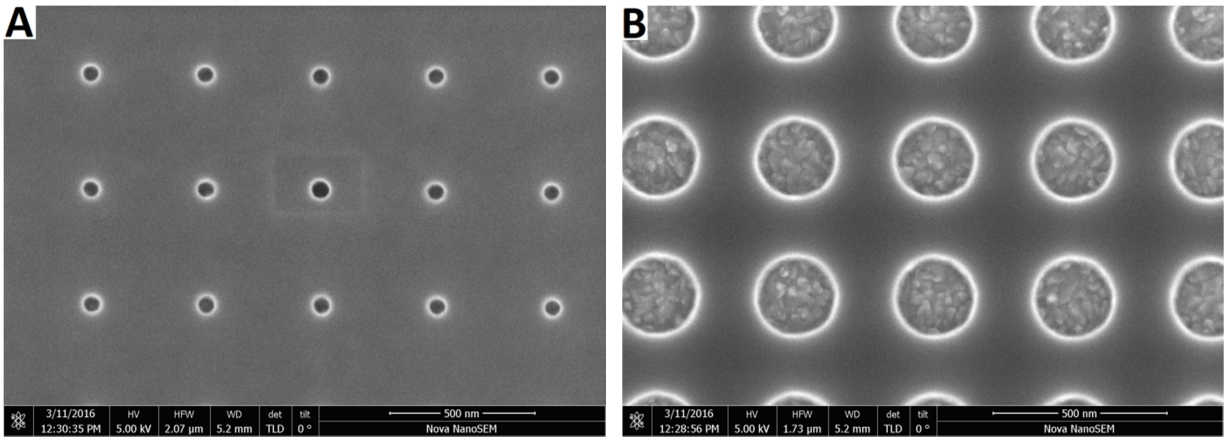

Figure 17: SEM image of the optimal dose (346 µC/cm^2) for the positive resist (pits), on the resist mask. A) the result for the 50 nm topography can be seen. B) the result for the 200 nm topography can be seen. For this topography there can be clearly seen that the holes are open, the underlying titanium grain structure is visible.

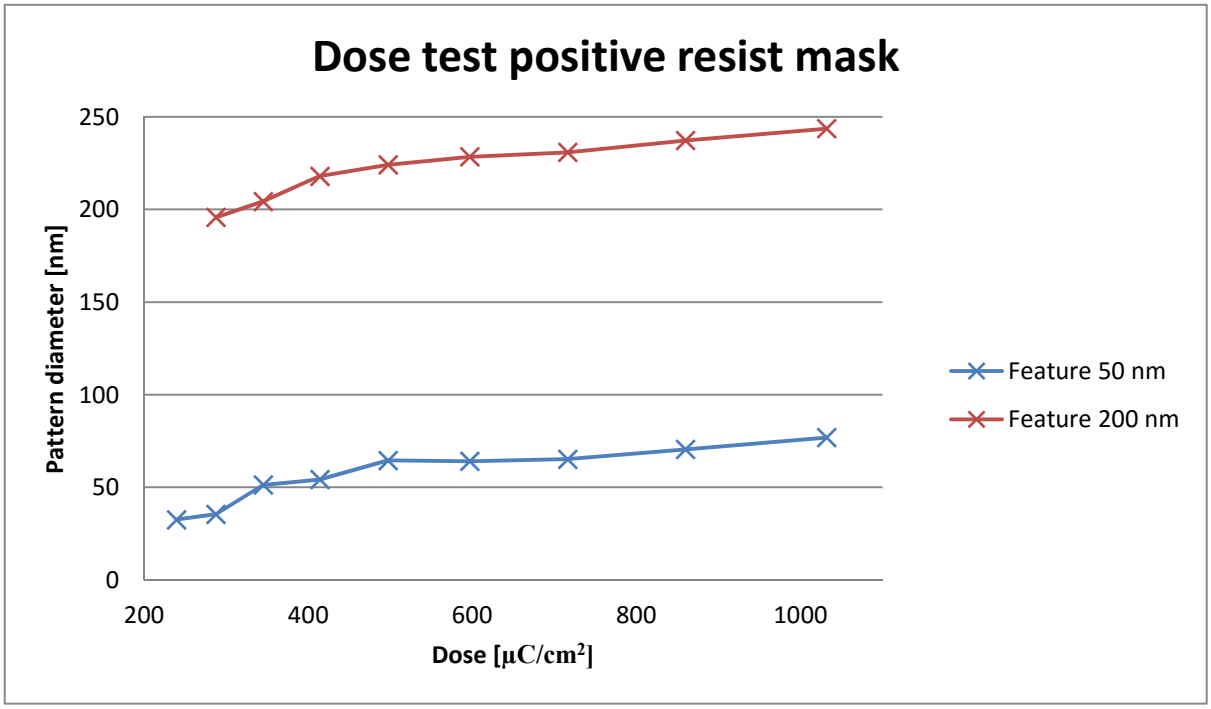

Figure 18: The effect of the applied dose on the diameter of the nanopatterns for the positive resist mask. The red line indicates the patterns of 200 nm in diameter, and the blue line indicates the patterns of 50 nm in diameter.

During the negative dose test, an error occurred on the 50 nm topography; the resist pillars collapsed. This collapse can be seen in Figure 19A. For the 200 nm pillars, the test results were positive and resist pillars were created. Based on this, it was determined that the dose was optimal at 3732 µC/cm^2. This was dose number 6. The SEM results can be seen in Figure 19B. In Appendix E – Dose Test Images (Figure 41), images are seen for the lowest and the highest dose. The difference between the doses can be seen in Figure 20. In this figure the measured diameters obtained from the dose test can be seen.

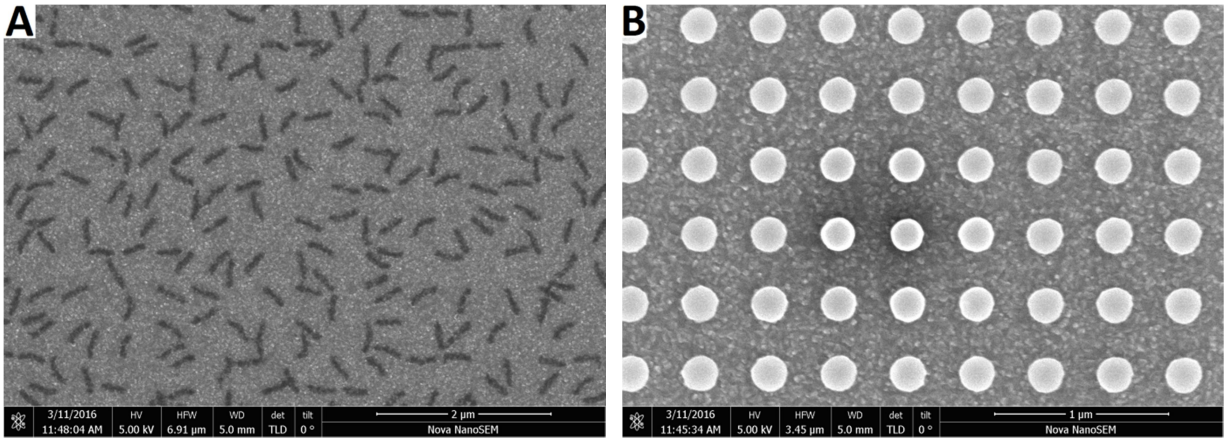

Figure 19: SEM image of the dose test for the negative resist (pillars) on the resist mask. A) The topography of the 50 nm resist pillars has collapsed. B) SEM image of the optimal dose (3732 µC/cm^2), for the 200 nm topography can be seen.

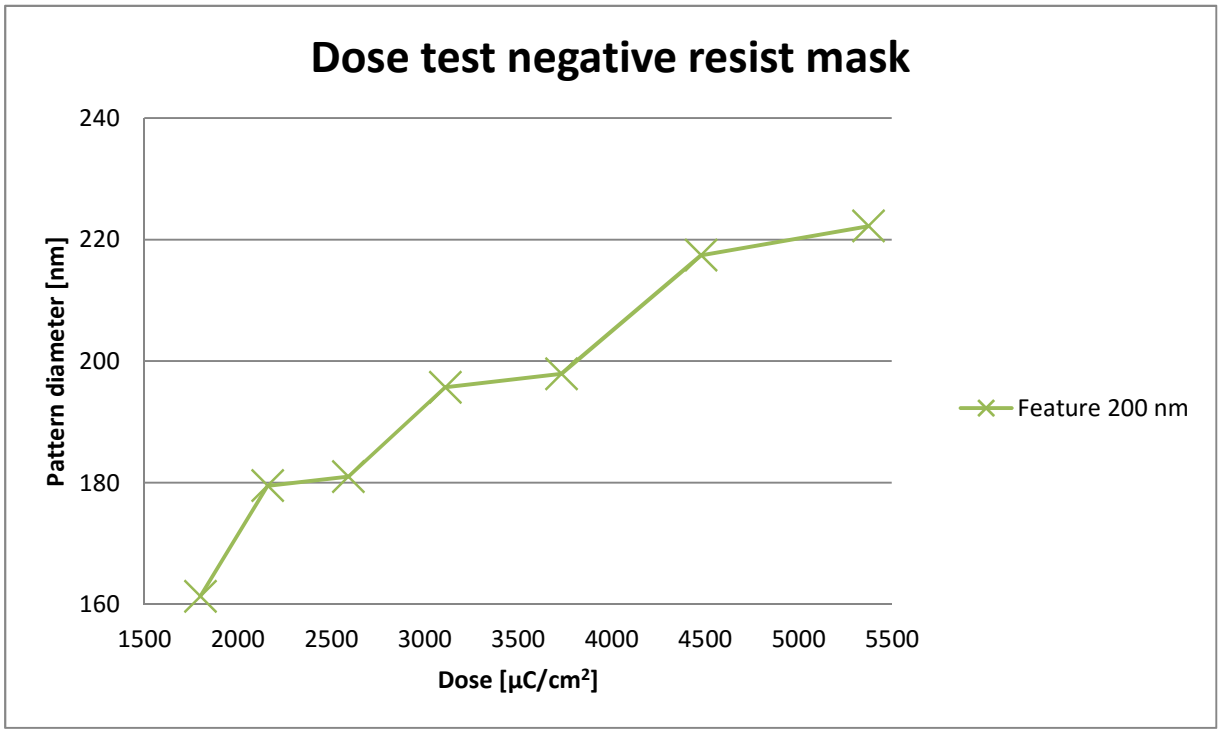

Figure 20: The effect of the applied dose on the diameter of the nanopatterns for the negative resist mask. The green line indicates the pattern of 200 nm in diameter.

3.2.2 Dose Test For The Hard Mask Process

The dose test for the hard mask is described in this section. During SEM inspection both the positive and the negative resist topography were studied. For the positive resist, the optimal dose was determined to be 288 µC/cm^2. This is dose number 3 during the dose test. The SEM results are seen in Figure 21. Within Figure 21A the 100 nm resist pits, and in Figure 21B, the 500 nm resist pits. In Appendix E – Dose Test Images (Figure 42 and Figure 43), images are seen for the lowest and the highest dose. The difference between the doses can be seen in Figure 22. In this figure the measured diameters from the dose test can be seen.

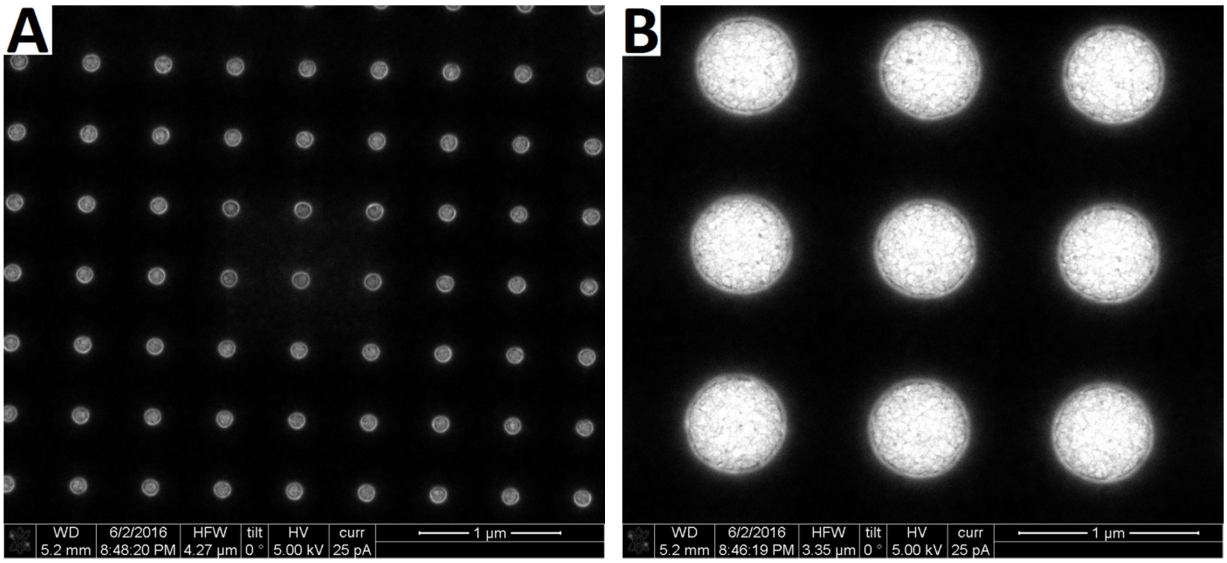

Figure 21: SEM image of the optimal dose (288 µC/cm^2) for the positive resist, on the hard mask. A) The result for the 100 nm topography can be seen. B) The result for the 500 nm topography can be seen.

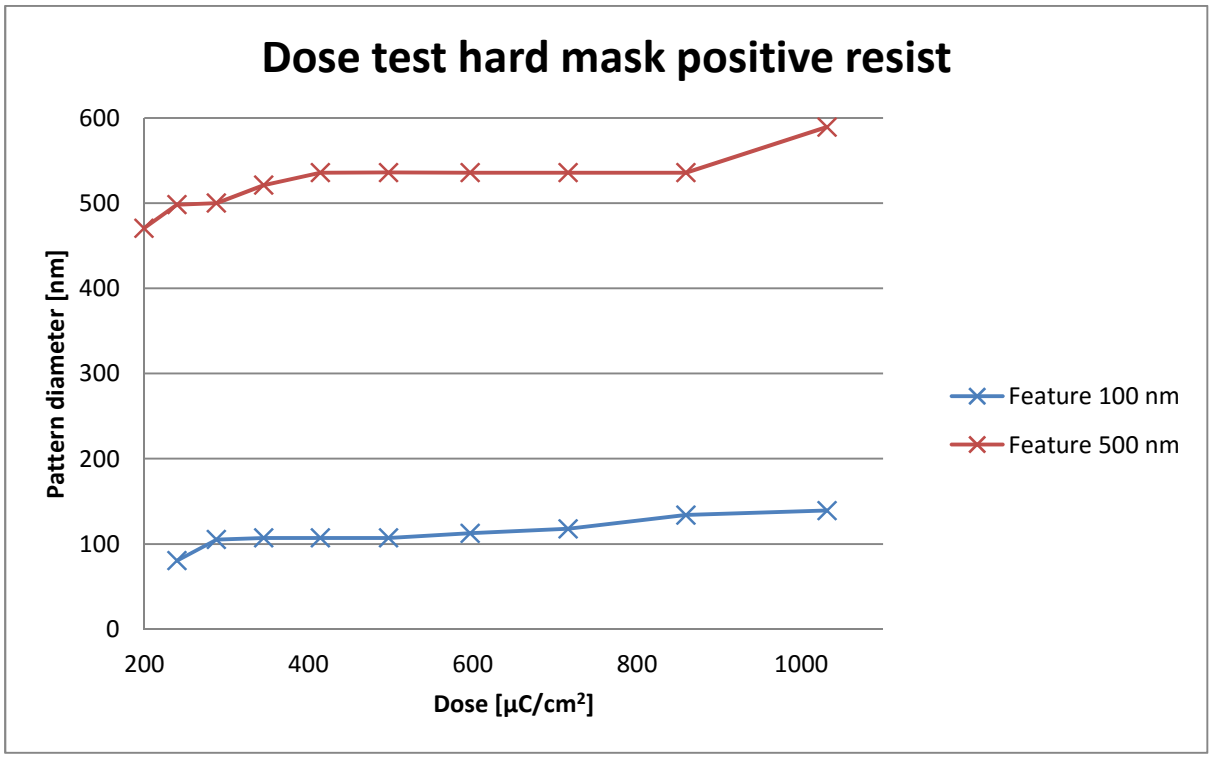

Figure 22: The effect of the applied dose on the diameter of the nanopatterns for the positive resist mask. The red line indicates the pattern of 500 nm in diameter, and the blue line indicates the pattern of 100 nm in diameter.

The results for the negative resist of the hard mask can be seen in Figure 23. There is only a result on the 500 nm structures. As there can be seen in Figure 23, the pillars are not in square order anymore. This was due to a resist attachment problem. However, on the 500 nm pillars was determined that the optimal dose for the negative resist on the hard mask is 3537 µC/cm^2 (dose number 10).

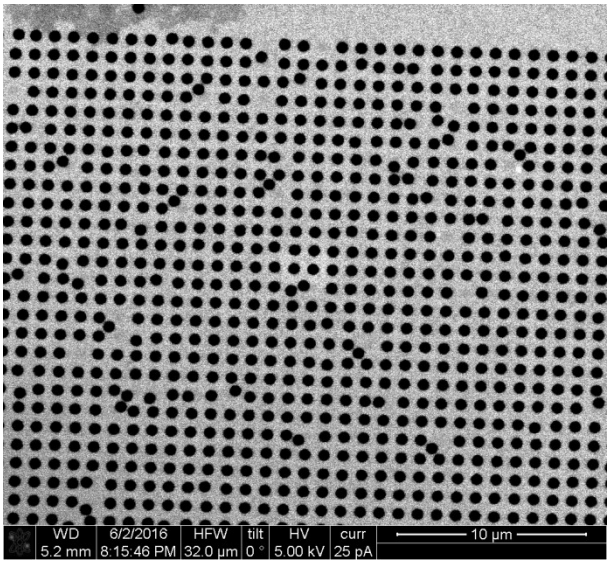

Figure 23: SEM image for the negative resist at the optimal dose (3537 µC/cm^2) for the hard mask. The pillars of 500 nm should have been in a square array. However the resist had attachment problems, and therefore some pillars have shifted.

3.3 Pattern Transfer

The pattern transfer was performed by two different methods, namely by reactive ion etching and ion milling. The results for etching can be seen in section 3.3.1, and the results for the ion milling can be seen in section 3.3.2. A summary for all results is seen in Table 5.

Table 5: Summary of the results obtained during etching. The numbers correspond to the etching recipes used, as numbered in section 2.3.

Recipe No.	Resist mask		Hard mask	
	Positive resist	Negative resist	Positive resist	Negative resist
1	-	Etched structure is black and very rough	-	-
2	Both pattern and resist gone	Both pattern and resist gone	-	-
3	Isotropic result for 60 s, however not reproducible	Not reproducible	-	-
4	Good result, not reproducible	Not reproducible	-	-
5	Both pattern and resist gone	Both pattern and resist gone	-	-
6	Both pattern and resist gone	Both pattern and resist gone	-	-
7	Both pattern and resist gone	Both pattern and resist gone	-	-
8	Both pattern and resist gone	Both pattern and resist gone	-	-
9	Both pattern and resist gone	Both pattern and resist gone	-	-
10	Isotropic etch results for positive resist	-	-	-
11	Both pattern and resist gone	Both pattern and resist gone	Good results	Results
12	-	Good results from 200 nm diameter	-	-
13	-	-	Aluminium oxide removal	Aluminium oxide removal
14	-	-	Aluminium removal to create mask	Aluminium removal to create mask
15	-	-	Aluminium hard mask removal	Aluminium hard mask removal

3.3.1 Reactive Ion Etching

During etching several recipes were used, as can be seen in Table 3 (section 2.3). The summary of the results, on the use of these recipes is displayed in Table 5. The results of the etching are described below.

For etch recipe number one, which was the Cl_2 and Ar etch. The resulting pattern (pits) can be seen in Figure 24. The inspection was performed by SEM. There can be seen that the structures, exposed to the chlorine and argon etch gas, have become very rough. By optical microscope inspection, these patterns appeared black.

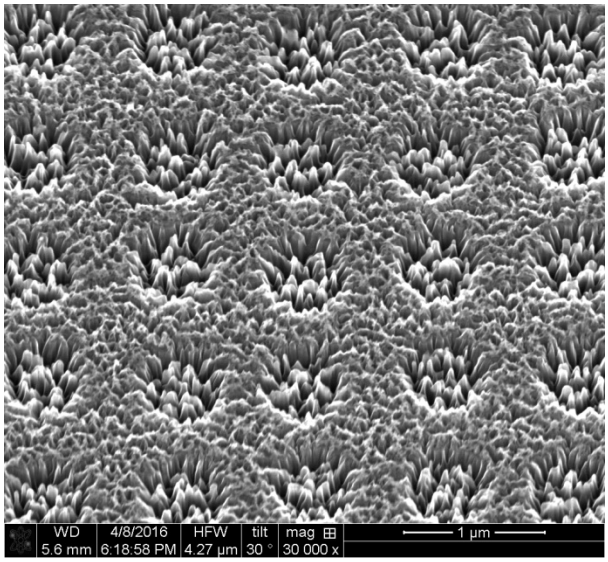

Figure 24: SEM image of the Cl_2 and Ar etch, recipe number one. In this image, the roughness inside the pits can be seen. The pits are 500 nm in diameter, as intended.

For the third etching recipe, which was CF_4, the SEM inspection result can be seen in Figure 25. The etchant for this recipe was CF_4, and the result was an isotropic etch, from which pits were obtained. However, this etching result was not reproducible, neither in the positive, nor in the negative resist.

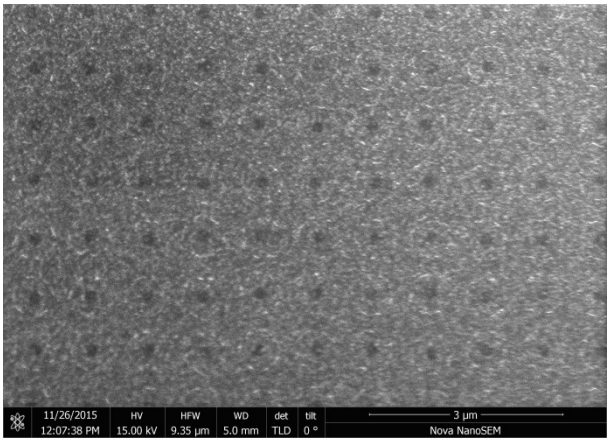

Figure 25: Image of the SEM inspection for CF_4, etching recipe three. Isotropic etching can be seen, as the pits of 100 nm in diameter became 240 nm in diameter.

The SEM inspection results for the fourth etching recipe CF_4 with O_2, can be seen in Figure 26. A pattern of 100 nm pits can be seen with an interspace distance of 900 nm, both are as intended. However, again this result was not reproducible.

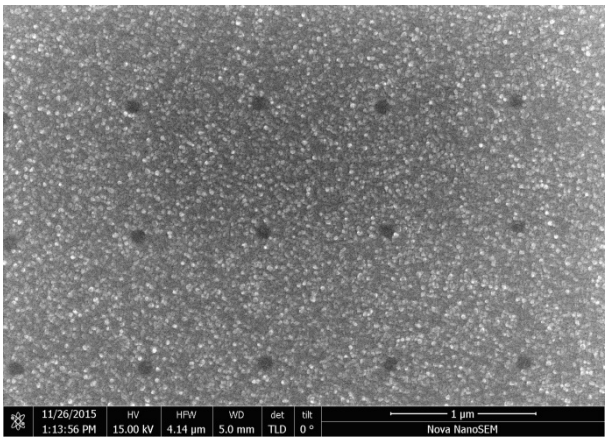

Figure 26: SEM inspection of CF_4 and O_2 etching, recipe number four. The topography pit diameter is 100 nm and the interspacing is 900 nm, as intended. However, this result was not reproducible.

The CHF_3 and Ar results of recipe number ten, obtained from SEM inspection can be seen in Figure 27. Isotropic etching was seen with this recipe. The intended diameter of the pit pattern was 200 nm. However, a diameter of 400 nm was measured during inspection.

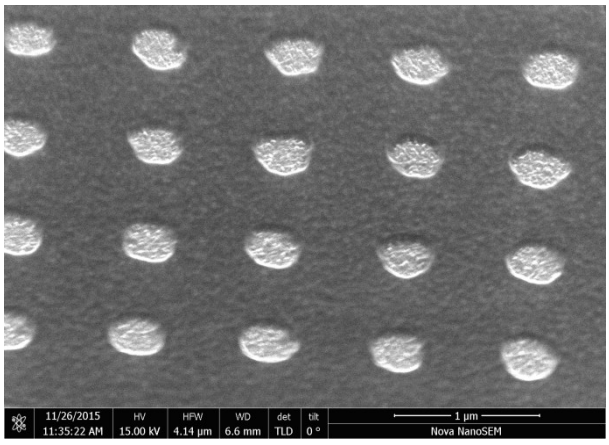

Figure 27: SEM inspection of the CHF_3 and Ar etching, recipe number ten. The intended topography pit diameter was 200 nm, the measured diameter was 400 nm.

The eleventh and final etching experiment on titanium, was with SF_6, CHF_3, and O_2. For this recipe two different results were obtained. With only the resist as a mask, both the resist and the pattern were gone within one minute, for both the positive and the negative resist mask. However, when the hard mask was applied, the titanium was etched. SEM inspection was performed, and the results were obtained on both the positive resist, and the negative resist.

On the positive resist in combination with the hard mask, the experiment was executed twice to test the reproducibility of the method. There are results on two different diameters, which can be seen in Figure 28 and in Figure 29. In Figure 28 the intended pit diameter was 500 nm. There can be see that in Figure 28A a pit diameter of 690 nm was measured, and in Figure 28B a diameter of 700 nm was measured. These results are larger than expected, hence isotropic etching was obtained. The edges of both topographies look similar, both are rounded. Since this structure could be reproduced twice, it is considered reproducible.

In Figure 29 the intended pit diameter was 100 nm. However, in Figure 29A a pit diameter of 313 nm was obtained and in Figure 29B a pit diameter of 326 nm was obtained. These results are also larger than expected, which also means that isotropic etching was

obtained. It can also be seen that the features look very similar on both topographies, they both look semi-spherical. Also this structure could be reproduced twice exactly the same, so it is also considered reproducible.

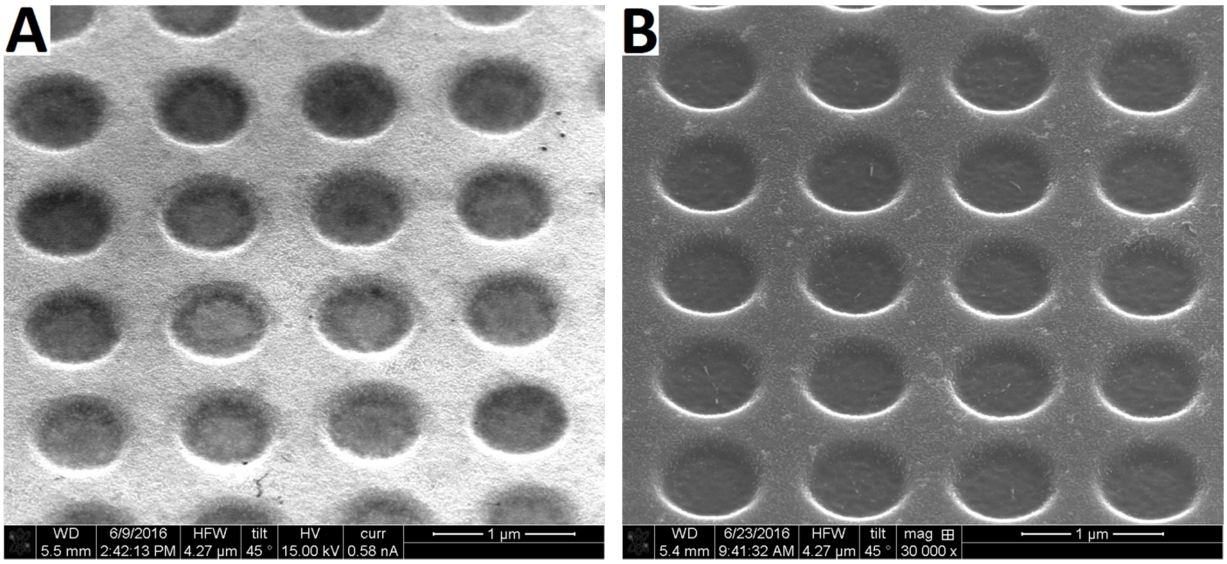

Figure 28: SEM inspection for etching of the positive resist on the hard mask, with SF_6, CHF_3, and O_2, recipe number eleven. For both designs, the intended pit diameter was 500 nm. A) the first experiment can be seen, the measured pit diameter was 690 nm. The conditions were isotropic. B) The second, repeat experiment can be seen. The measured pit diameter was 700 nm, hence the conditions were also isotropic. However, the pits are very similar to the first experiment seen in A.

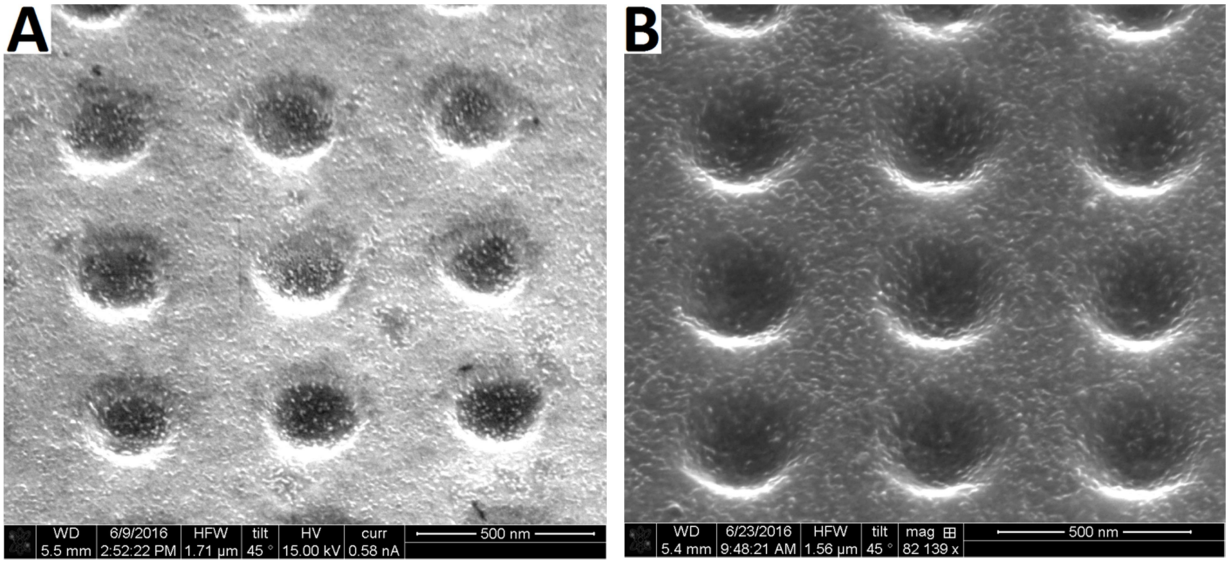

Figure 29: SEM inspection for etching of the positive resist on the hard mask, with SF_6, CHF_3, and O_2, recipe number eleven. For both designs, the intended pit diameter was 100 nm. A) the first experiment can be seen, the measured pit diameter was 313 nm. The conditions were isotropic. B) The second, repeat experiment can be seen. The measured pit diameter was 326 nm, hence the conditions were also isotropic. However, the pits are very similar to the first experiment seen in A.

For the negative resist on the hard mask, the specimen was obtained from the RIE equipment with very little to no titanium left on the wafer. However, the larger markers were still optically visible. Since the top of the wafers, just below the titanium, was non-conductive, a thin layer of gold (4 nm) was deposited onto the wafer to enhance the conductive properties of the wafer, such that it could be inspected by SEM. The resulting images can be seen in

Figure 30. From the dose test results (section 3.2.2), it was already known that there is an attachment problem of the resist to the structure. This attachment problem is still visible after etching, since the resist was the mask to etch the aluminium. This is seen by the displacement from the square position of the topography.

In Figure 30A, the first experiment on the hard mask with the negative resist can be seen. The intended pillar diameter was 500 nm, however a pillar diameter of 395 nm was obtained. The etching has been too deep, since the titanium was gone except for the patterns. In Figure 30B, the reproduction of the first experiment can be seen. Again the intended pillar diameter was 500 nm, however a pillar diameter of 368 nm was measured. This diameter is slightly smaller than the diameter obtained during the first run. The topography for this second experiment is even more distributed, this means that the resist attachment problems were more severe compared to the first experiment. For both Figure 30A and Figure 30B the pattern features were very similar. The pillars could be created twice, hence this method is reproducible. However, the resist attachment problems are very severe. Due to these attachment problems there were no results obtained on the 100 nm features during the dose test, hence it was not possible to have a result on etching.

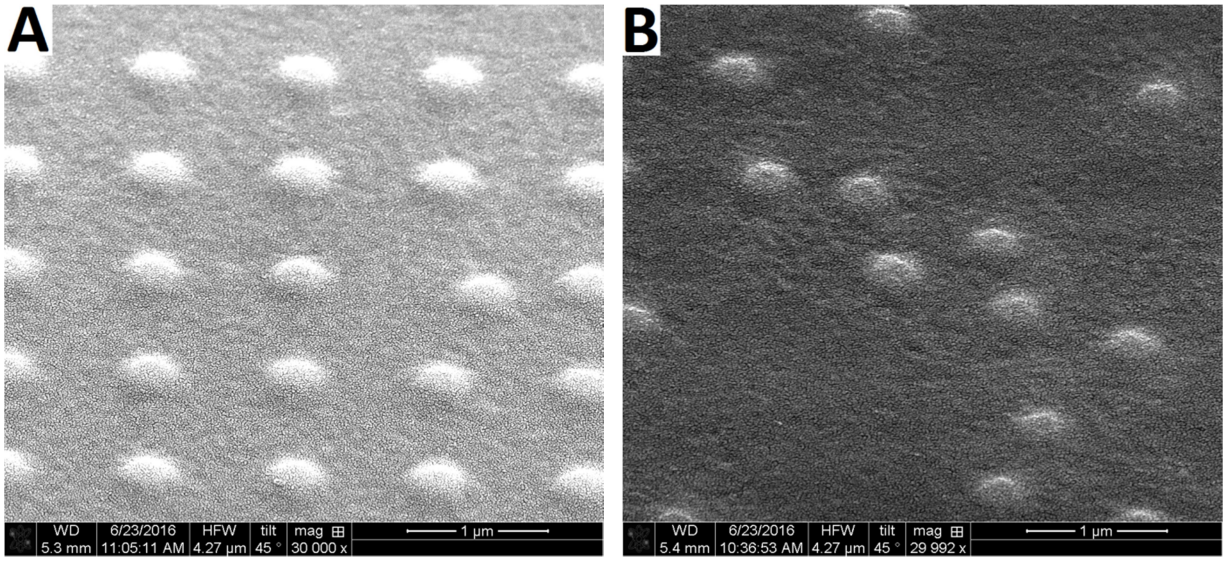

Figure 30: SEM inspection for etching of the of the negative resist on the hard mask, with SF_6, CHF_3, and O_2, recipe number eleven. For both designs, the intended pillar diameter was 100 nm. A) The first experiment, a slight resist attachment problem was seen. The measured pillar diameter was 395 nm. The etching was isotropic. B) The second, repeat experiment can be seen. The resist attachment problem was more severe than during the first experiment. The measured pillar diameter was 368 nm. However, the pillars are very similar to the pillars seen in the first experiment.

3.3.2 Ion Milling

The patterns created by ion milling, were also imaged by a SEM. There were two different etching times used during this process, 150 s and 300 s. 150 s was used to create the topography with a smaller diameter, 200 nm. 300 s was used to pattern the large features of 500 nm. The results obtained were reproducible, for both topographies. On diameters lower than 200 nm no reproducible result was obtained.

The results for the 200 nm pillar diameter can be seen in Figure 31. In Figure 31A the first experiment with these conditions is seen, and in Figure 31B the reproduction of the first process can be seen. From the design, there is known that the pillars should be 200 nm in diameter, however in the results there can be seen that a pillar diameter of 245 nm was

obtained. Both the first experiment and the reproduction lead to the same result for the feature size and shape. The height as measured by SEM inspection was for both procedures about 50 nm.

The results for the pillars of 500 nm in diameter, were obtained by using an etching time of 300 s. The results obtained from SEM inspection can be seen in Figure 32. As there can be seen, the structures are not equal. The first experiment has semi-spherical features, and the reproduction has pillars that are flat on top. The flat top was intended during the experiment. However, the pillar diameter obtained is equal. The first experiment was intended to have pillar diameter of 500 nm, and this became 545 nm. The reproduction was also intended to have pillar diameter of 500 nm, and this also became 545 nm. The height of the topography was measured 100 nm in both structures during SEM inspection.

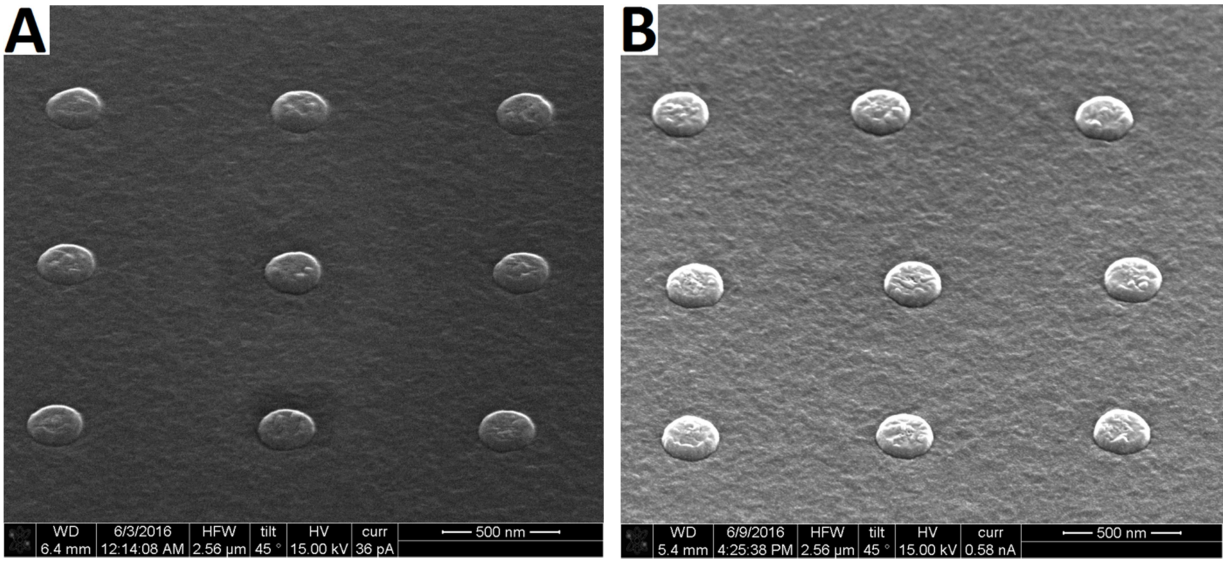

Figure 31: SEM inspection of ion milling, on the 200 nm pillar pattern. A) The pillars of 200 nm in diameter during the first experiment, the pillar diameter became 245 nm after ion milling. B) The reproduction of the process on the same pillar diameters, also this 200 nm topography became 245 nm.

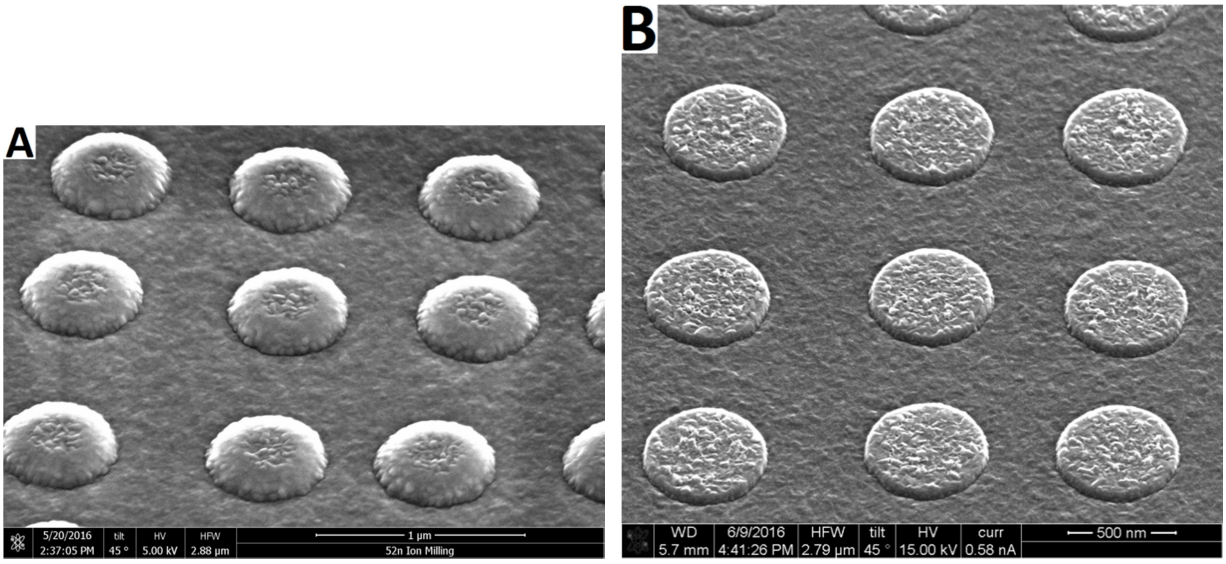

Figure 32: SEM results of the 300 s ion milling pillars. A) The semi-spherical first experiment can be seen, the intended pillar diameter was 500 nm, 545 nm was measured. B) The flat-top reproduction can be seen, the intended pillar diameter was 500 nm, 545 nm was measured.

4 Discussion

The main parameters determined during this study were the dose test parameters and the etching parameters. Firstly, the effect of the dose on the resultant pattern is discussed (section 4.1). Secondly the pattern transfer by RIE and ion milling is discussed (section 4.2). In Figure 33 the two results for both processes can be seen.

4.1 Effect of the Dose on the Resultant Patterns

For the dose test several different doses were used. In Table 6 the optimal doses for each resist substrate combination are seen. During literature research, no notation of a dose test was found. However, the dose is a main patterning parameter. From the dose test, it is seen that the pattern diameter obtained differed with every different dose (as seen in Figure 18, Figure 20, and Figure 22). During SEM inspection, these patterns were measured and the optimal dose was chosen.

Table 6: Summary for the optimal doses obtained from the dose test

Resist mask		Hard mask	
Positive resist dose [$\mu C/cm^2$]	**Negative resist dose [$\mu C/cm^2$]**	**Positive resist dose [$\mu C/cm^2$]**	**Negative resist dose [$\mu C/cm^2$]**
346	3732	288	3537

The doses for each substrate and resist combination differ. This difference can be explained from the substrate-resist interactions. The substrate underneath the resist of the hard mask consists out of aluminium. The substrate underneath the resist of the resist mask consists out of titanium. This difference between these substrates, leads to a difference in the forward scattering and back scattering. The forward scattering range is in the order of 1-10 nm, and is dependent on the resist characteristics and the acceleration voltage. Since the layer thickness of the resists are the same, and the same settings are used, the forward scattering does not give an explanation for the changing dose between the hard mask and the resist mask. Back scattering occurs due to electrons travelling into the substrate, and these electrons scatter on contact with the substrate. In this way, the back scattered electrons contribute to the exposure of the resist, in a range of ~10 µm. Since in both substrates, the material underneath the resist are different, the electrons travelling through these different substrates also behave differently. Therefore, the change in the dose with the same resist can be explained, by the back scattered electrons.

The difference in dose between the positive and the negative resist can be explained by the difference in resist type. The positive resist, is formed from cross-linked polymers. These polymer bonds are broken by the electron beam during EBL. A prescribed amount of energy is needed to break the bonds. The negative resist is formed out of polymer parts. These parts are cross-linked by the electron beam during EBL. A prescribed amount of energy is needed to form the polymer bonds. Both energies differ from each other, due to the difference in polymer molecules, and the different energy needed to break or form the bonds [26].

Using the optimal dose, the features can be patterned in the exact shape and size required. However, not only the dose is important. During this study, it became apparent that also the resist thickness must be chosen carefully to pattern the topography. During the dose test the 50 nm pillars collapsed (see Figure 19A). These pillars collapsed, due to the high aspect ratio of the height of the pattern (the resist thickness) to the pattern diameter. To avoid this pillar collapse, a thinner resist layer had to be chosen during the patterning of the design. The dose with this thinner layer of resist did not change. This was due to the contribution of

the scattering effects, as mentioned before. Most contribution of the scattering effects was due to the back scattering, and not due to the resist.

Due to this high aspect ratio and the pillar collapse, the pattern diameter of 30 nm and 50 nm had to be excluded from the design. These diameters would result in a resist mask that would have been 30 nm thin. Such a thin resist mask is a disadvantage during etching. The mask would etch away before any pattern was transferred. This means that the topography of 30 nm and 50 nm in diameter were replaced. For the replacement, the smallest and largest pattern diameters were chosen 100 nm and 500 nm.

For the hard mask [25] the silicon dioxide layer, and the aluminium layer had to be adjusted to suit the designed pattern sizes. There was taken into account that, the aspect ratio of the aluminium mask was kept as low as possible, without compromising the mask properties, to enhance the etching capabilities. The thickness of the total hard mask was lowered to 48 nm (8 nm SiO_2 and 40 nm Al). This was possible due to the inertness of the aluminium to the fluorine gas. This inertness resulted in a mask that was resistant to the used titanium etch, but not to the aluminium etch. The etching methods can be seen in Table 7 (recipe number 11, 13, 14, and 15).

During the dose test for the hard mask, also a problem with the attachment of the negative resist to the substrate occurred. This attachment problem should have been solved by the use of HMDS as an attachment layer. Due to this attachment problem, the results for the hard mask are only obtained on the larger (500 nm) structures. The smaller structures, detached from the surface during development of the resist. It is recommended to try and use AR 300-80 as a primer for the negative resist, to enhance the attachment of the negative resist. This primer has recently become available, and should take care of the resist attachment problem.

4.2 Pattern Transfer by Reactive Ion Etching and Ion Milling

To transfer the pattern into the titanium etching methods were used. Two different etching methods were used RIE and ion milling. During etching, also several different recipes were used. The chosen recipes can be seen in Table 7. Recipe number 11 was used with RIE, and recipe number 12 was used with ion milling.

The RIE experiments that use only resist as an etching mask display poor results. Etching recipe number one [31,32], with Cl_2 and Ar, gave a very rough result on the etched bottom. This roughness was black under the optical microscope. The black appearance, combined with the very rough surface, looks similar to silicon black. In silicon black it is assumed that there is a local variation in the etch rate at the surface, this variation leads to localised etching. When etching is continued the side walls of the structure will become non-reactive, and the etching is continued deep into the structure [34]. It is assumed that a similar process occurred on the titanium, during the Cl_2 and Ar etch. However, from literature [31,32], it was noted that these conditions would lead to a smooth surface.

For the third etching recipe using only CF_4, the tenth recipe using CHF_3 and Ar, and the eleventh recipe [25] using SF_6, CHF_3, and O_2, isotropic etching conditions were obtained. Isotropic conditions mean that the wrong gas is used, or the composition of the used gas should be changed. Also, recipe number three and number ten are not reproducible. Hence, these were discarded as etching methods.

For recipe number eleven isotropic etching conditions can be avoided (using SF_6, CHF_3, and O_2) [25]. To avoid isotropy and obtain anisotropy, the gas flow rates needs to be tuned, in the same way like Löffler et al. [25] studied. During this study it was assumed that the optimal flow rates used by Löffler et al. [25] had the correct composition and was transferable to the equipment in the Kavli laboratory. However, it was noted that when these conditions are used, a different result is obtained. This difference can be explained by the

different equipment used. Every piece of equipment has a slight variation when compared. The flow rates of the gases used can differ slightly. There is however not only a variation between the used machine brands, but there is also a slight difference between two machines of the same brand.

For recipe number eleven, also an aluminium wet etch was needed to remove the remaining aluminium mask. It was noted, that during the aluminium wet etch [30], the etch rate given was not reached. The aluminium wet etch was very slow. It is considered that this is due to the aluminium oxide on the surface of the mask. It is assumed that this aluminium oxide layer significantly lowers the etch rate of the aluminium wet etch, hence a longer etching time was needed than subscribed.

To image the results for etching on the negative hard mask a layer of gold was needed to enhance the imaging. This means that the non-conductive layer below the titanium was seen. It was seen that the etching duration was to long for the negative hard mask. The layer of titanium, except for the pattern, was etched away. This was not intended, the etching rate was higher than expected from Löffler et al. [25]. With a shorter time, and a better gas composition, pillars in the titanium substrate can be obtained.

From ion milling the only reproducible pattern with a resist mask was obtained. During ion milling the diameters of the topography became larger than the designed diameter. This change in diameter was obtained from the ion bombardment. During the ion bombardment, the titanium particles that were etched away were not evaporated into the gas mixture, but these were deposited at a different place on the surface (section 2.3). In this case, the bombarded titanium was deposited against the resist patterns and against the already obtained patterns, thereby enlarging the diameter of the pattern.

Further, it was noted that there are no results on patterns smaller than 200 nm. To obtain the 200 nm patterns the etching time was decreased from 300 s to 150 s. This decrease in time, also reduced the pillar height to half the original height. This decrease, is due to the etching rate. During both processes the same gas conditions were used, therefore the same etching rate is obtained. This means that when the time is reduced, the height is also reduced in an equal amount.

Table 7: Summary of the optimal etching parameters.

Recipe No.	**Gases [sccm]**			**Power [W]**	**Bias [V]**	**Time [s]**	**Ref.**
11	13 SF_6	13 CHF_3	15 O_2	100	-280	180	[25]
12	30 Ar			100	-675	150, 300	Experience

In Figure 33 the smallest obtained patterns can be seen for the two production methods. First the evaporated film titanium can be seen. On the titanium, the hard mask process in combination with RIE, or the ion milling process is applied. After the application of the process, both patterns as seen are obtained.

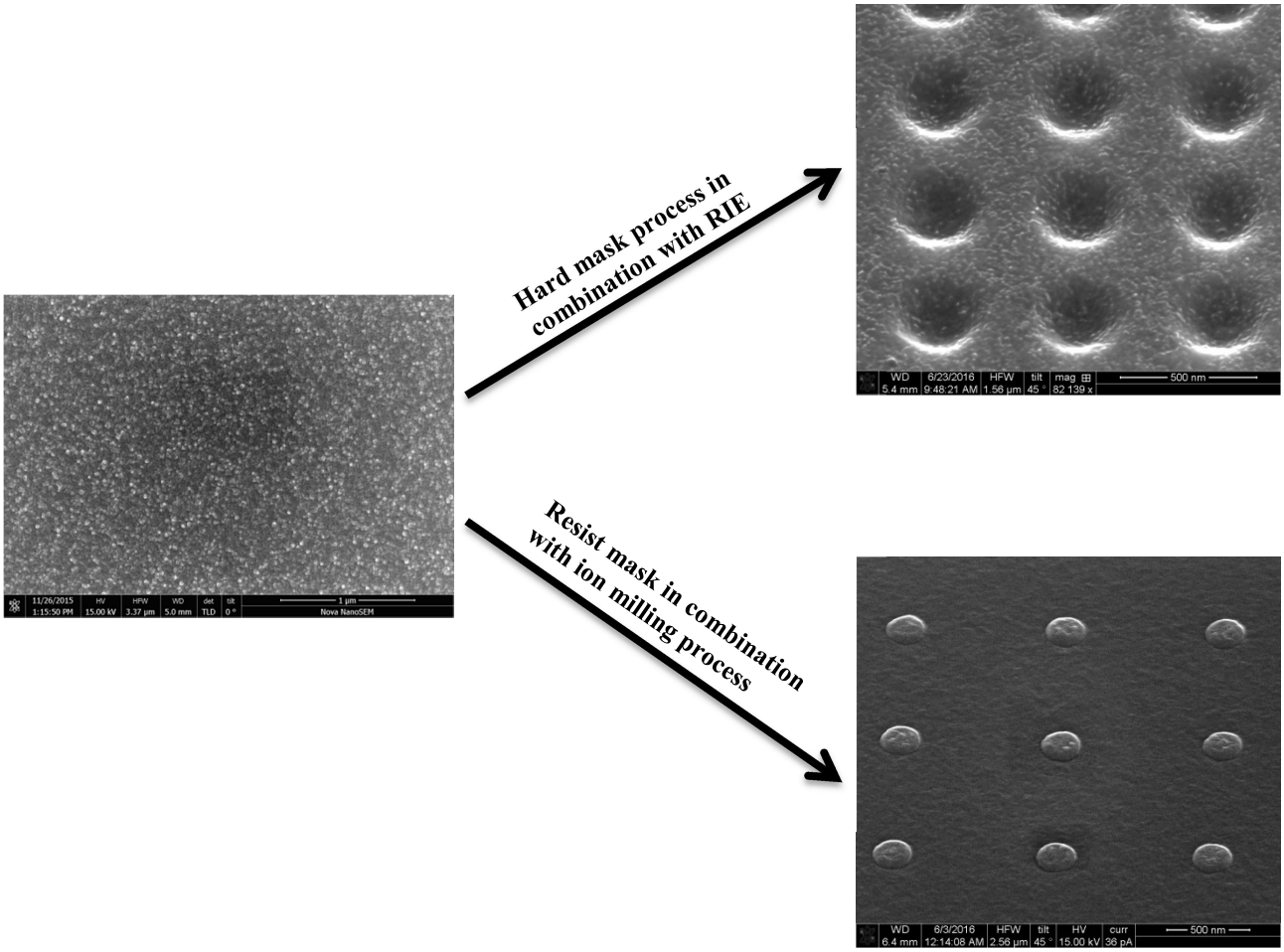

Figure 33: The resultant patterns on the thin film titanium substrate for the two processes created by the hard mask in combination with RIE and the resist mask in combination ion milling.

5 Conclusions and Recommendations

During this research, two methods for nanopatterning of a titanium substrate have been developed. With both methods, EBL was applied for precision patterning using a resist and a hard mask after which etching was performed to transfer the pattern into the titanium.

To obtain precision patterning a dose test was needed. This dose test was performed for both the resist mask and the hard mask. For the resist mask, the doses obtained are 346 $\mu C/cm^2$ for the positive resist, and 3732 $\mu C/cm^2$ for the negative resist. For the hard mask the doses obtained are 288 $\mu C/cm^2$ for the positive resist, and 3537 $\mu C/cm^2$ for the negative resist.

For the negative resist with the hard mask, an attachment problem for the resist was encountered. During this study HMDS was used as a primer for attachment, however this does not work properly. It is recommended to try and use AR 300-80 as a primer for the negative resist, to enhance the attachment of the negative resist.

The hard mask designed consisted out of a thin layer of silicon dioxide and a layer of aluminium. This hard mask was used as an etching mask during RIE. This led to favourable etching conditions. Patterns were obtained that are 320 nm and 700 nm in pit diameter, and pillars of 395 nm in diameter.

Since the hard mask gave very good results during etching, and it did not etch in fluorine gas, it is recommended to use the hard mask instead of a resist mask during fluorine RIE procedures. With the hard mask fluorine etching can be applied, which was not possible with the resist mask only.

The etching for the hard mask was isotropic. It is recommended to tune the gas composition for the machinery in the Kavli laboratory, to obtain anisotropic etching. The results on the negative hard mask, also show that the titanium is completely removed, except for the pillars. It is recommended to lower the etching time, to create the pattern completely into the titanium surface.

The other patterning method found, was based on the use of a resist mask and ion milling. It was found that the etching time was dependent on the topography. The patterns that were created are pillars of 245 nm and 545 nm in diameter.

It is recommended to perform more research on the different pattern feature sizes with both methods developed. With the improved methods, all desired nanopatterns could be created and biological research can then be performed onto these patterns, to determine the optimal pattern for MSC differentiation into osteoblasts.

When this study is compared to previous studies, it is noted that a new EBL process has been developed for patterning titanium in the submicron to nanoscale. A process that offers control to the pattern features with these scales, where the topography design can be easily changed, and this topography is transferred into titanium. Previous research offered precision control into polymers, or patterns with relatively little control into titanium.

6 Acknowledgements

This project could not have finished without the help of several people. In this chapter I would like to thank the people who helped me during the thesis.

First of all I would like to thank Carel Heerkens, he was of great importance for me inside the Kavli laboratory. He taught me how to use most machines in this laboratory. Second I would like to thank Lidy Fratila-Apachitei and Kees Hagen, who have supervised me for the past year. They also offered lots of advice about the experiments. Last I would like to thank the other technicians from the Kavli laboratory, and the material science laboratory, that offered help during my project.

Also I would like to thank my family and friends, for their support.

7 References

[1] W. Chen, Y. Shao, X. Li, G. Zhao and J. Fu, "Nanotopographical surfaces for stem cell fate control: Engineering mechanobiology from the bottom," *Nanotoday,* no. 8, pp. 759-784, 2015.

[2] A. Carrel and M. Burrows, "Cultivation in vitro of malignant tumors," *The Journal of Experimental Medicine,* pp. 571-575, 1911.

[3] C. Chen, M. Mrksich and G. Huang, "Geometric control of cell life and death," *Science,* pp. 1425-1428, 1997.

[4] C. Wilkinson, M. Riehle, M. Wood, J. Gallagher and A. Curtis, "The use of materials patterned on a nano- and micro-metric scale in cellular engineering," *Materials Science & Engineering,* no. 19, pp. 263-269, 2002.

[5] M. Wood, D. Meredith and F. Owen, "Step toward a model nanotopography," *IEEE Transactions on Bionanoscience,* vol. 1, no. 4, pp. 133-140, 2002.

[6] A. Wilkinson, R. Hewitt, L. McNamara, D. McCloy, R. Meek and M. Dalby, "Biomimetic microtopography to enhanceosteogenesis in vitro," *Acta Biomaterialia,* no. 7, pp. 2919-2925, 2011.

[7] O. Zouani, C. Chanseau, B. Brouillard, R. Bareille, F. Deliane, M. Foulc, A. Mehdi and M. Durrieu, "Altered nanofeature size dictates stem cell differentiation," *Biomaterials,* no. 125, pp. 1217-1224, 2011.

[8] L. Prodanov, E. lamers, M. Domanski, R. Luttge, J. Jansen and X. Walboomers, "The effect of nanometric surface texture on bone contract to titanium implants in rabbit tibia," *Biomaterials,* no. 34, pp. 2920-2927, 2013.

[9] J. Kim, W. Bae, K. Lim, K. Jang, S. Oh, K. Jang, N. Jeon, K. Suh and J. Chung, "Density of nanopatterned surfaces for designing bone tissue engineering scaffolds," *Materials Letters,* no. 130, pp. 227-231, 2014.

[10] G. Abagnale, M. Steger, V. Nguyen, N. Hersch, A. Sechi, S. Joussen, B. Deneck, R. Merkel, B. Hoffmann, A. Dreser, U. Schnakenberg, A. Gillner and W. Wagner, "Surface topography enhances differentiation of mesenchymal stem cells towards osteogenic and adipogenic lineages," *Biomaterials,* no. 61, pp. 316-326, 2015.

[11] A. Hart, N. Gadegaard, C. Wilkinson, R. Oreffo and M. Dalby, "Osteoprogenitor response to low-adhesion nanotopographies originally fabricated by electron beam lithography," *Journal of Material Science: Materials in Medicine,* no. 18, pp. 1211-1218, 2007.

[12] M. Dalby, N. Gadegaard, R. Tare, A.Andar, M. Riehle, P. Herzyk, C. Wilkinson and R. Oreffo, "The control of human mesenchymal cell differentiation using nanoscale symmetry and disorder," *Nature materials,* no. 6, pp. 997-1003, 2007.

[13] N. Gadegaard, M. Dalby, M. Riehle and C. Wilkinson, "Optimizing substrate disorder for bone tissue engineering of mesenchymal stem cells," *Journal of Vacuum Science & Technology B,* no. 26, pp. 2554-2557, 2008.

[14] R. McMurray, N. Gadegaard, P. Tsimbouri, K. Burgess, L. McNamara, R. Tare, K. Murawski, E. Kinham, R. Oreffo and M. Dalby, "Nanoscale surfaces for long-term maintenance of mesenchymal stem cell phenotype and multipotency," *Nature Materials,* no. 10, pp. 637-644, 2011.

[15] A. Klymov, E. Bronkhorst, J. Riet, J. Jansen and X. Walboomers, "Bone marrow-derived mesenchymal cells feature selective migration behavior on submicro- and nano-dimensional multi-patterned substrates," *Acta Biomaterialia,* no. 16, pp. 117-125, 2014.

[16] T. Sjöström, M. Dalby, A. Hart, R. Tare, R. Oreffo and B. Su, "Fabrication of pillar-like titania nanostructures on titanium and their interactions with human skeletal stem cells," *Acta Biomaterialia,* no. 5, pp. 1433-1441, 2009.

[17] L. McNamara, T. Sjöström, K. Burgess, J. Kim, E. Liu, S. Gordonov, P. Moghe, R. Meek, R. Oreffo, B. Su and M. Dalby, "Skeletal stem cell physiology on functionally distinct titania nanotopographies," *Biomaterials,* no. 32, pp. 7403-7410, 2011.

[18] M. Dalby, D. McCloy, M. Robertson, H. Agheli, D. Sutherland, S. Affrossman and R. Oreffo, "Osteoprogenitor response to semi-ordered and random nanotopographies," *Biomaterials,* pp. 2980-2987, 2006.

[19] C. Berry, A. Curtis, R. Oreffo, H. Agheli and D. Sutherland, "Human fibroblast and human bone marrow cell response to lithographically nanopatterned adhesive domains on protein rejecting substrates," *IEEE Transsactions on Nanobioscience,* vol. 6, no. 3, pp. 201-209, 2007.

[20] J. Fiedler, B. Özdemir, J. Bartholomä, A. Plettl and R. Brenner, "The effect of substrate surface nanotopography on the behavior of multipotnent mesenchymal stromal cells and osteoblasts," *Biomaterials,* no. 34, pp. 8851-8859, 2013.

[21] A. Greer, K. Seunarine, A. Khokhar, X. Li, D. Moran and N. Gadegaard, "Direct nanopatterning of commercially pure titanium with ultra-nanocrystalline diamond stamps," *Physica Status Solidi A,* no. 9, pp. 1721-1725, 2012.

[22] A. Greer, K. Seunarine, A. Khokhar, I. MacLaren, A. Brydone, D. Moran and N. Gadegaard, "Increased efficiancy of direct nanoimprinting on planar and curved bulk titanium through surface modification," *Microelectronics Engineering,* pp. 67-73, 2013.

[23] C. Sittig, M. Textor, N. Spencer, M. Wieland and P. Vallotton, "Surface characterization of implant materials c.p. Ti, Ti-6Al-7Nb and Ti-6Al-4V with different pretreatments," *Journal of Material Science: Materials in Medicine,* no. 10, pp. 35-46, 1999.

[24] C. Deshpandey and R. Bunshah, Thin film processes II, San Diego: Academic Press, Inc. , 1991.

[25] R. Löffler, M. Fleischer and D. Kern, "An anisotropic dry etch process with fluorine chemistry to create well-defined titanium surfaces for biomedical studies," *Microelectronic engineering,* no. 97, pp. 361-364, 2012.

[26] C. Constancias, S. Landis, S. Manakli, L. Martin, L. Pain and D. Rio, Lithography, vol. Chapter 3. Electron Beam Lithography, Wiley, 2011.

[27] A. v. Langen-Suurling and A. v. Run, "Kavli Nanolab Delft cleanrooms home page," 02 07 2015. [Online]. Available: https://cleanroom.kavli.tudelft.nl/. [Accessed 01 10 2015].

[28] G. Oehrlein, Handbook of Plasma Processing Technology - Fundamentals, Etching, Deposition, and Surface Interactions, Vols. Chapter 8 - Reactive Ion Etching, New Jersey: Noyes Publications, 1990.

[29] M. Domanski, R. Luttge, E. Lamers, X. Walboomers, L. Winnubst, J. Jansen and J. Gardeniers, "Submicron-patterning of bulk titanium by nanoimprint lithography and reactive ion etching," *Nanotechnology,* no. 23, pp. 1-12, 2012.

[30] K. Williams, K. Gupta and M. Wasilik, "Etch Rates for Micromachining Processing - Part II," *Journal of Microelectromechanical systems,* vol. 12, no. 6, pp. 761-778, 2003.

[31] E. Parker, B. Thibeault, M. Aimi, M. Rao and N. MacDonald, "Inductively Coupled Plasma Etching of Bulk Titanium," *Journal of the electrochemical society,* no. 10, pp. C675-C683, 2005.

[32] O. Khandan, M. Kahook and M. Rao, "Fenestrated microneedles for ocular drug

delivery," *Sensors and Actuators B223,* pp. 15-23, 2016.

[33] I. Hotovy, I. Kostic, S. Hascik, V. Rehacek, M. Predanocy and A. Bencurova, "Patterning of titanium oxide surface using inductively coupled plasma for gas sensing," *Applied Surface Science,* no. 312, pp. 107-111, 2014.

[34] S. Kalem, P. Werner, Ö. Arthursson, V. Talalaev, B. Nilsson, M. Hagberg, H. Frederisen and U. Södervall, "Black silicon with high density and high aspect ratio nanowhiskers," *Nanotechnology,* vol. 22, no. 23, 2011.

Appendix A – Controlled disorder

To create the controlled disorder, a MATLAB file was written. In this appendix the MATLAB code is given.

```
% Random pattern coordinate generation for the disordered patterns
close all;
clear all;
clc;

% Declaration of variables
cc = 45 ;                            % The centre-to-centre distance in nm
disorder = 7.5 ;                       % The disorder in nm
degree = randi(360,10) ;              % The direction of the disorder per dot
x_dev = zeros(10,10) ;                % The deviation in x
y_dev = zeros(10,10) ;                % The deviation in y
% x- and y-coordinates in square arrangement
x = [ 0 , cc , 2*cc , 3*cc , 4*cc , 5*cc , 6*cc , 7*cc , 8*cc , 9*cc ;
      0 , cc , 2*cc , 3*cc , 4*cc , 5*cc , 6*cc , 7*cc , 8*cc , 9*cc ;
      0 , cc , 2*cc , 3*cc , 4*cc , 5*cc , 6*cc , 7*cc , 8*cc , 9*cc ;
      0 , cc , 2*cc , 3*cc , 4*cc , 5*cc , 6*cc , 7*cc , 8*cc , 9*cc ;
      0 , cc , 2*cc , 3*cc , 4*cc , 5*cc , 6*cc , 7*cc , 8*cc , 9*cc ;
      0 , cc , 2*cc , 3*cc , 4*cc , 5*cc , 6*cc , 7*cc , 8*cc , 9*cc ;
      0 , cc , 2*cc , 3*cc , 4*cc , 5*cc , 6*cc , 7*cc , 8*cc , 9*cc ;
      0 , cc , 2*cc , 3*cc , 4*cc , 5*cc , 6*cc , 7*cc , 8*cc , 9*cc ;
      0 , cc , 2*cc , 3*cc , 4*cc , 5*cc , 6*cc , 7*cc , 8*cc , 9*cc ;
      0 , cc , 2*cc , 3*cc , 4*cc , 5*cc , 6*cc , 7*cc , 8*cc , 9*cc ] ;
y = [ 9*cc , 9*cc , 9*cc , 9*cc , 9*cc , 9*cc , 9*cc , 9*cc , 9*cc , 9*cc ;
      8*cc , 8*cc , 8*cc , 8*cc , 8*cc , 8*cc , 8*cc , 8*cc , 8*cc , 8*cc ;
      7*cc , 7*cc , 7*cc , 7*cc , 7*cc , 7*cc , 7*cc , 7*cc , 7*cc , 7*cc ;
      6*cc , 6*cc , 6*cc , 6*cc , 6*cc , 6*cc , 6*cc , 6*cc , 6*cc , 6*cc ;
      5*cc , 5*cc , 5*cc , 5*cc , 5*cc , 5*cc , 5*cc , 5*cc , 5*cc , 5*cc ;
      4*cc , 4*cc , 4*cc , 4*cc , 4*cc , 4*cc , 4*cc , 4*cc , 4*cc , 4*cc ;
      3*cc , 3*cc , 3*cc , 3*cc , 3*cc , 3*cc , 3*cc , 3*cc , 3*cc , 3*cc ;
      2*cc , 2*cc , 2*cc , 2*cc , 2*cc , 2*cc , 2*cc , 2*cc , 2*cc , 2*cc ;
      cc , cc , cc , cc , cc , cc , cc , cc , cc , cc ;
      0 , 0 , 0 , 0 , 0 , 0 , 0 , 0 , 0 , 0 ] ;

%Calculate the x- and y-coordinates
for i = 1:10
    for j = 1:10

        % Calculating the disorders in relative x and y direction
        if degree(i,j) == 0
            x_dev(i,j) = 0 ;
            y_dev(i,j) = disorder ;
        elseif degree(i,j) == 90
            x_dev(i,j) = disorder ;
            y_dev(i,j) = 0 ;
        elseif degree (i,j) == 180
            x_dev(i,j) = 0 ;
            y_dev(i,j) = -disorder ;
        elseif degree(i,j) == 270 ;
            x_dev(i,j) = -disorder ;
            y_dev(i,j) = 0 ;
        elseif degree(i,j) == 360
            x_dev(i,j) = 0 ;
            y_dev(i,j) = disorder ;
        elseif degree(i,j) < 90
            x_dev(i,j) = sind(degree(i,j)) * disorder ;
```

```
            y_dev(i,j) = cosd(degree(i,j)) * disorder ;
        elseif degree(i,j) < 180
            deg = degree(i,j) - 90 ;
            x_dev(i,j) = cosd(deg) * disorder ;
            y_dev(i,j) = (sind(deg) * disorder) * -1 ;
        elseif degree(i,j) < 270
            deg = degree(i,j) - 180 ;
            x_dev(i,j) = (sind(deg) * disorder) * -1 ;
            y_dev(i,j) = (cosd(deg) * disorder) * -1 ;
        elseif degree(i,j) < 360
            deg = degree(i,j) - 270 ;
            x_dev(i,j) = (cosd(deg) * disorder) * -1 ;
            y_dev(i,j) = sind(deg) * disorder ;
        end
    end
end

% Round of values at nm
x_dev = round(x_dev) ;
y_dev = round(y_dev) ;

% Put the first circle without disorder to ease the drawing process
x_dev(10,1) = 0 ;
y_dev(10,1) = 0 ;

% Calculate the exact positions in x- and y-direction
x = x + x_dev ;
y = y + y_dev ;

% Write data to excel to store
file = 'coordinates.xlsx' ;
xlswrite(file,x,1,'B2:K11') ;
xlswrite(file,y,1,'B13:K22') ;
```

Appendix B – Patterns

Table 8: All patterns chosen for the first experiment.

Number	Pattern code	Diameter [nm]	Interspacing [nm]	Disorder [nm]
1	30/300/00	30	300	0
2	30/300/15	30	300	15
3	30/300/30	30	300	30
4	30/300/50	30	300	50
5	30/300/75	30	300	75
6	30/900/00	30	900	0
7	30/900/15	30	900	15
8	30/900/30	30	900	30
9	30/900/50	30	900	50
10	30/900/75	30	900	75
11	50/300/00	50	300	0
12	50/300/15	50	300	15
13	50/300/30	50	300	30
14	50/300/50	50	300	50
15	50/300/75	50	300	75
16	50/900/00	50	900	0
17	50/900/15	50	900	15
18	50/900/30	50	900	30
19	50/900/50	50	900	50
20	50/900/75	50	900	75
21	100/300/00	100	300	0
22	100/300/15	100	300	15
23	100/300/30	100	300	30
24	100/300/50	100	300	50
25	100/300/75	100	300	75
26	100/900/00	100	900	0
27	100/900/15	100	900	15
28	100/900/30	100	900	30
29	100/900/50	100	900	50
30	100/900/75	100	900	75
31	200/300/00	200	300	0
32	200/300/15	200	300	15
33	200/300/30	200	300	30
34	200/300/50	200	300	50
35	200/900/00	200	900	0
36	200/900/15	200	900	15
37	200/900/30	200	900	30
38	200/900/50	200	900	50
39	200/900/75	200	900	75
40	300/900/00	300	900	0
41	300/900/15	300	900	15
42	300/900/30	300	900	30

43	300/900/50	300	900	50
44	300/900/75	300	900	75
45	500/900/00	500	900	0
46	500/900/15	500	900	15
47	500/900/30	500	900	30
48	500/900/50	500	900	50
49	500/900/75	500	900	75

Appendix C – Dose Test Design

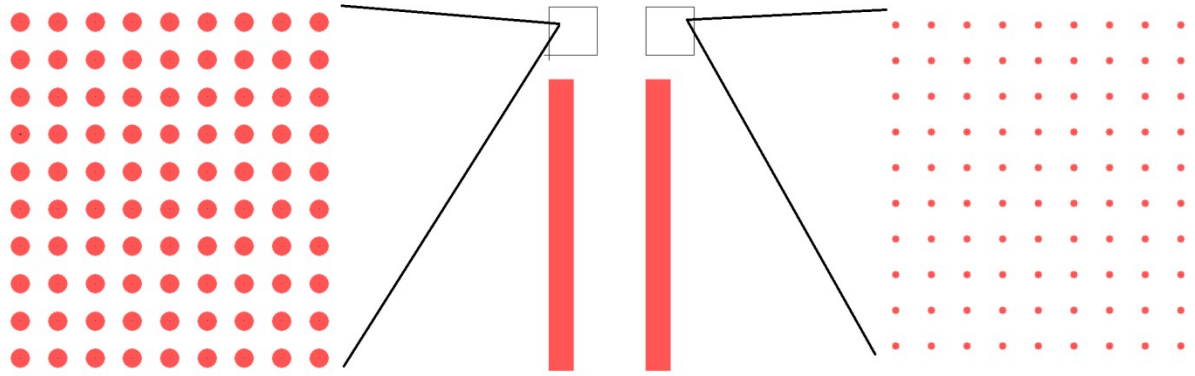

Figure 34: The design used for the dose test, on the hard mask. On the left the dots of 500nm can be seen and on the right the dots of 100nm can be seen.

Appendix D – Roughness measurements

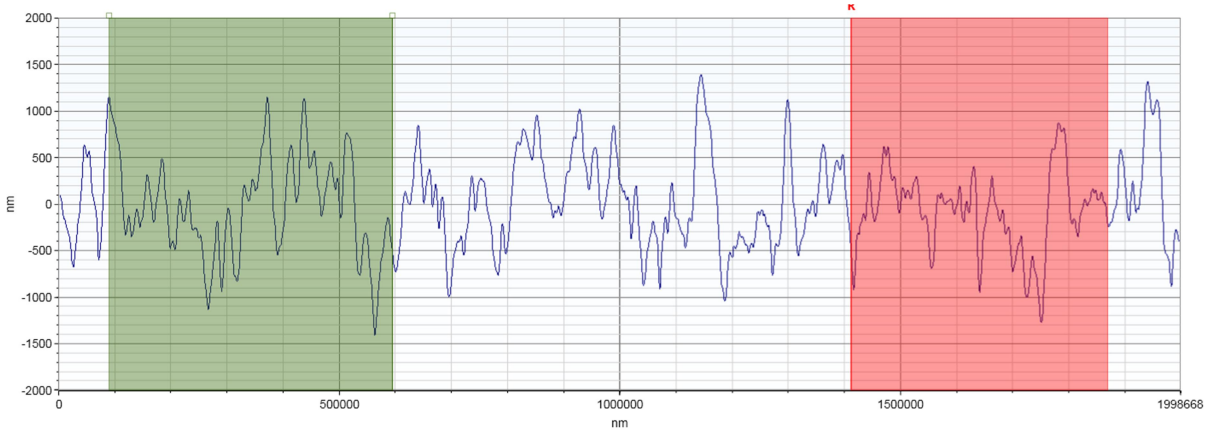

Figure 35: Roughness measurement of the DektakXT on the commercially pure titanium disc as delivered. Ra = 352 nm.

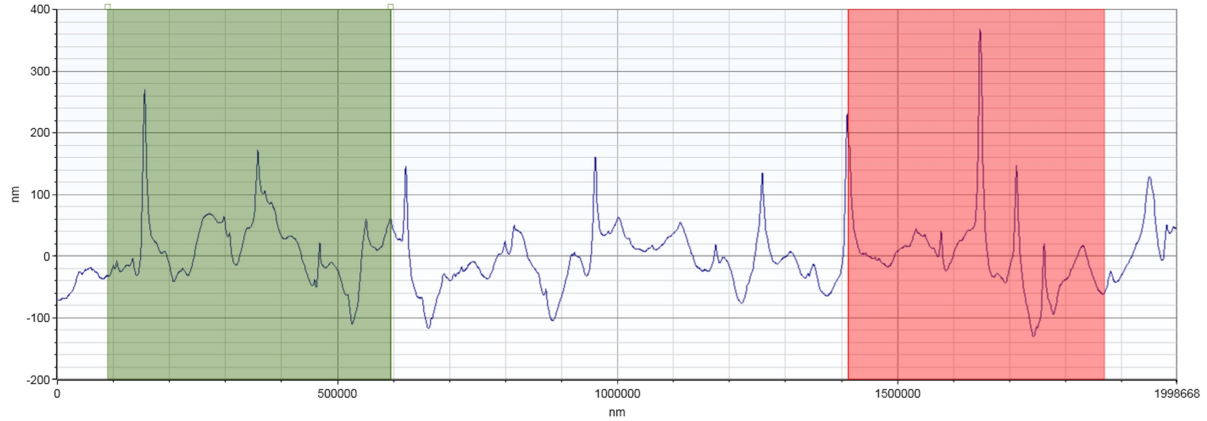

Figure 36: Roughness measurement of the DektakXT on the manually polished commercially pure titanium discs. Ra = 61.5 nm.

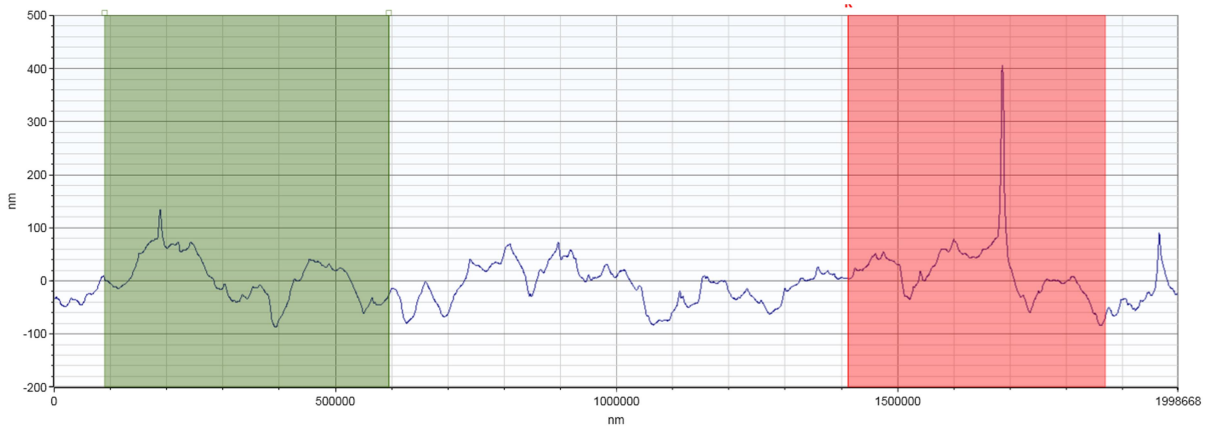

Figure 37: Roughness measurement of the DektakXT on the automatically polished commercially pure titanium discs. Ra = 28.6 nm.

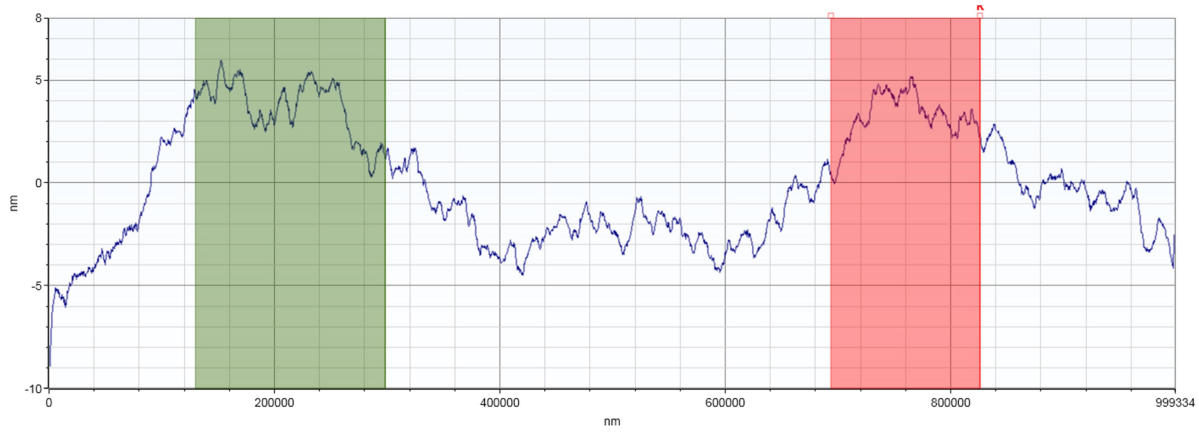

Figure 38: Roughness measurement of the DektakXT on the evaporated titanium. Ra = 3.8 nm.

Appendix E – Dose Test Images

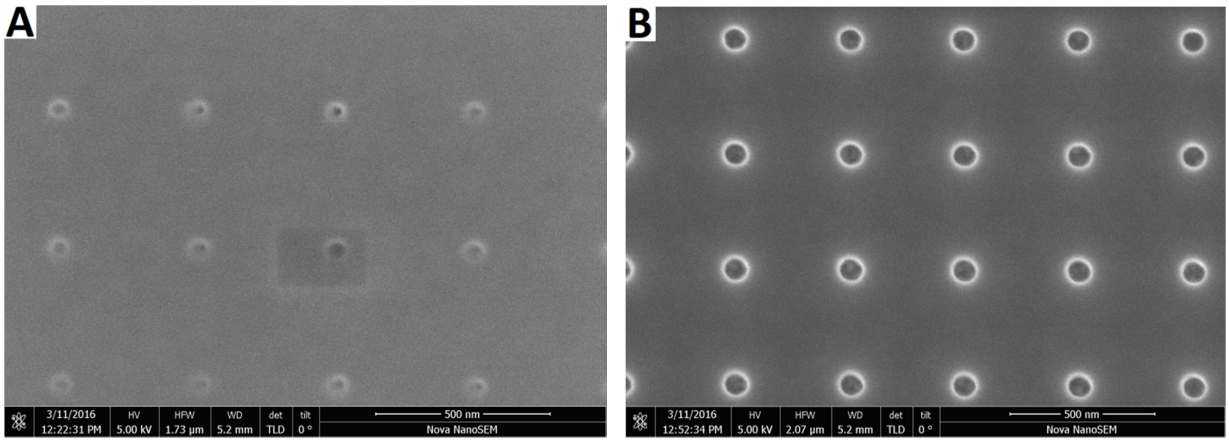

Figure 39: Dose test on the positive resist mask, 50 nm features. A) Dose number 2 from the dose test. There can be seen that the resist is not open up to the titanium, also the pits are only 32.6 nm in diameter. B) Dose number 10 from the dose test. The holes are completely open, however the diameter is 76.9 nm.

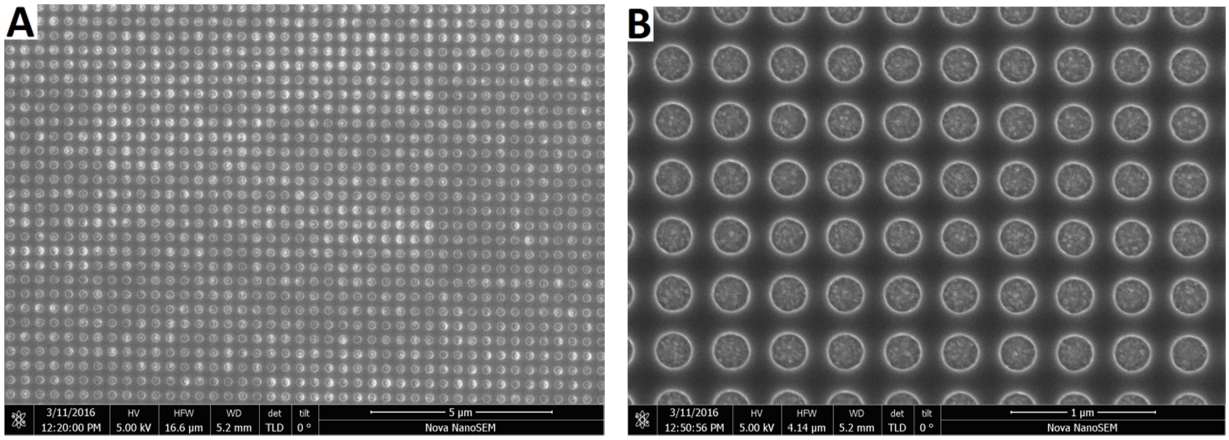

Figure 40: Dose test on the positive resist mask, 200 nm features. A) Dose number 2 from the dose test. There can be seen that the resist is not open up to the titanium, also the pits are only 190 nm in diameter. B) Dose number 10 from the dose test. The holes are completely open, however the diameter is 244 nm.

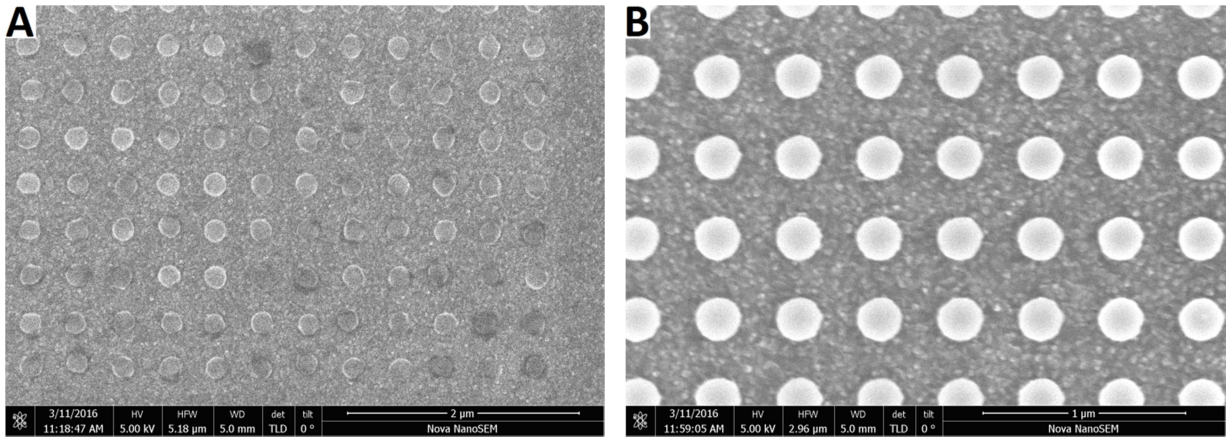

Figure 41: Dose test on the positive negative mask, 200 nm features. A) Dose number 2 from the dose test. There can be seen that there are no clear pillars, also the pillars are only 161 nm in diameter. B) Dose number 8 from the dose test. The holes are completely open, however the diameter is 222 nm.

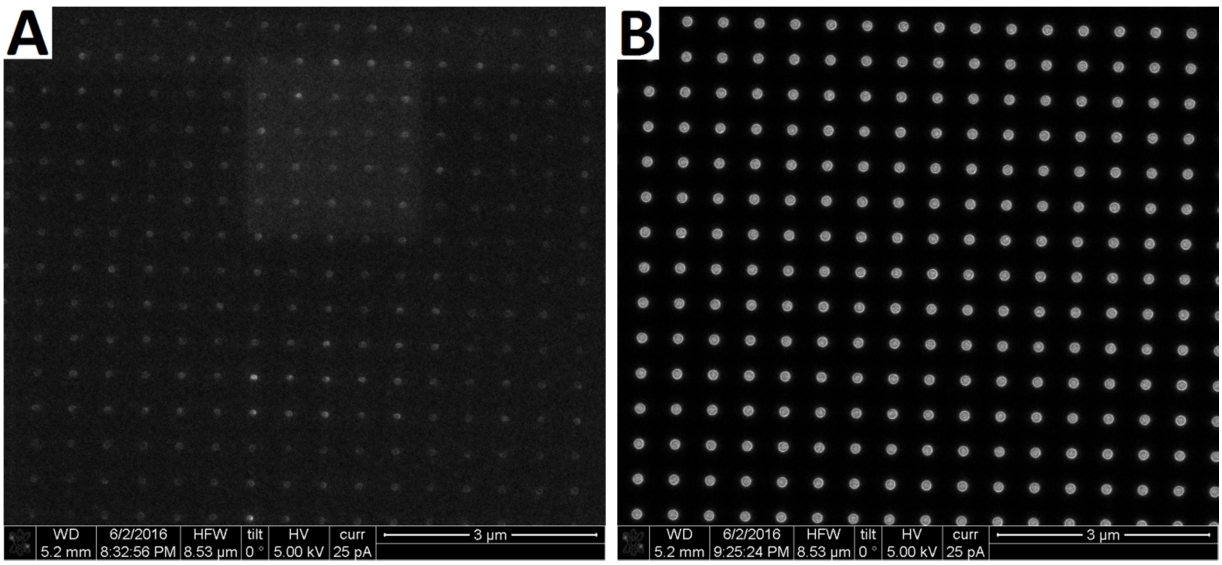

Figure 42: Dose test for the positive hard mask, 100 nm features. A) Dose number 1 from the dose test. There can be seen that the resist is not opened up to the titanium, also the pits are only 80.4 nm in diameter. B) Dose number 10 from the dose test. The holes are completely open, however the diameter is 139 nm.

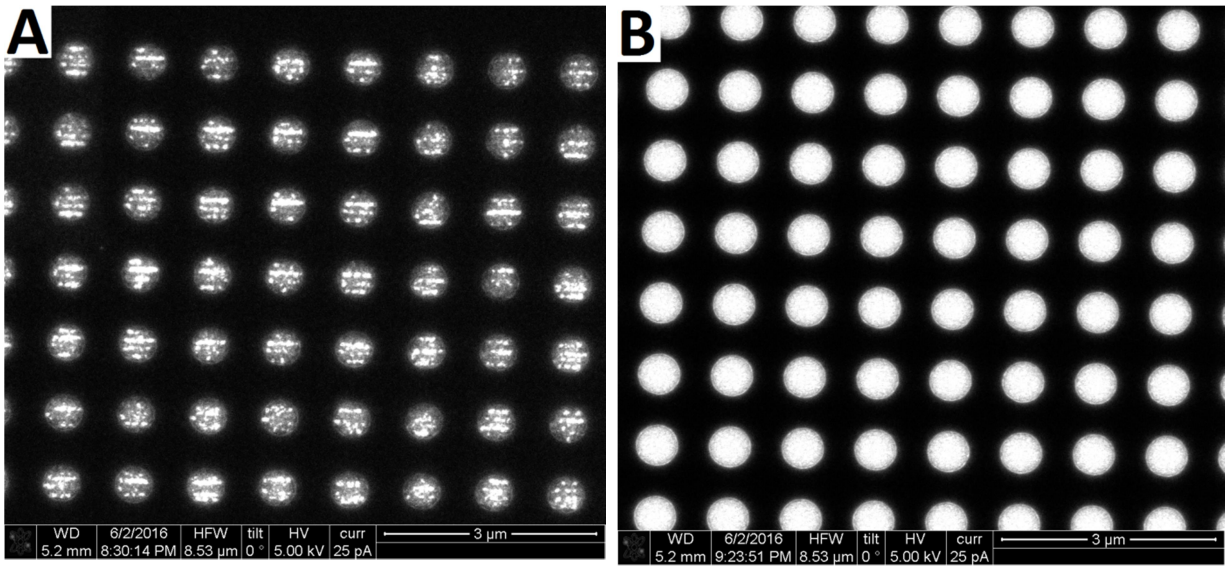

Figure 43: Dose test for the positive hard mask, 500 nm features. A) Dose number 1 from the dose test. There can be seen that the resist is not opened up to the titanium, also the pits are only 471 nm in diameter. B) Dose number 10 from the dose test. The holes are completely open, however the diameter is 589 nm.

Appendix F – Overview Images of the Patterns

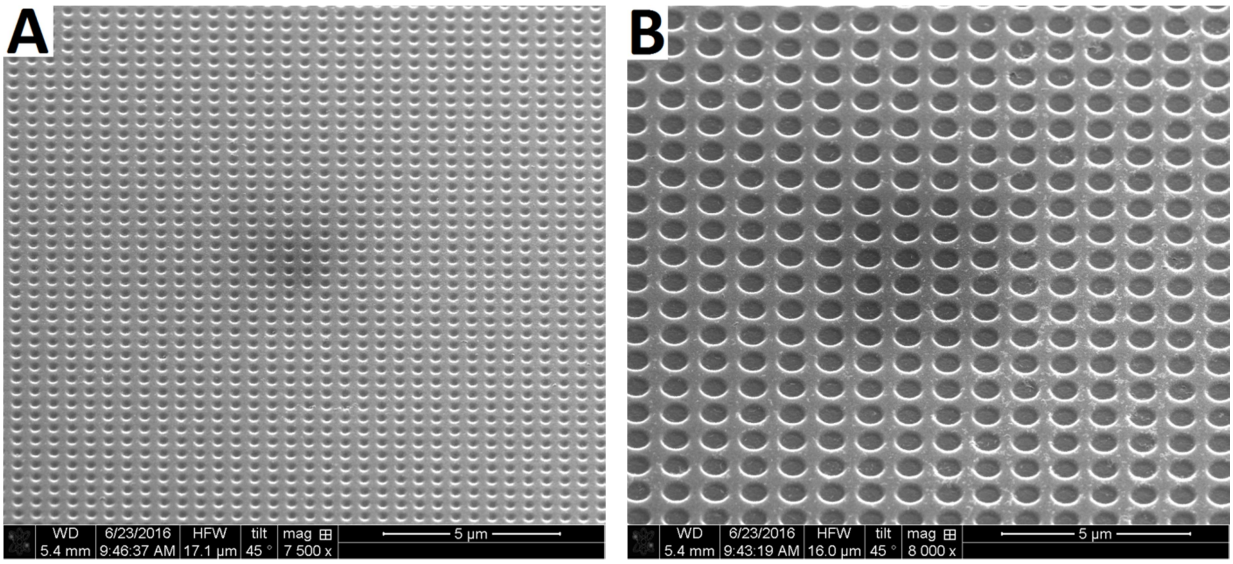

Figure 44: Overview image of part of the pattern created with the hard mask method A) An overview of the 320 nm pits. B) An overview of the 700 nm pits.

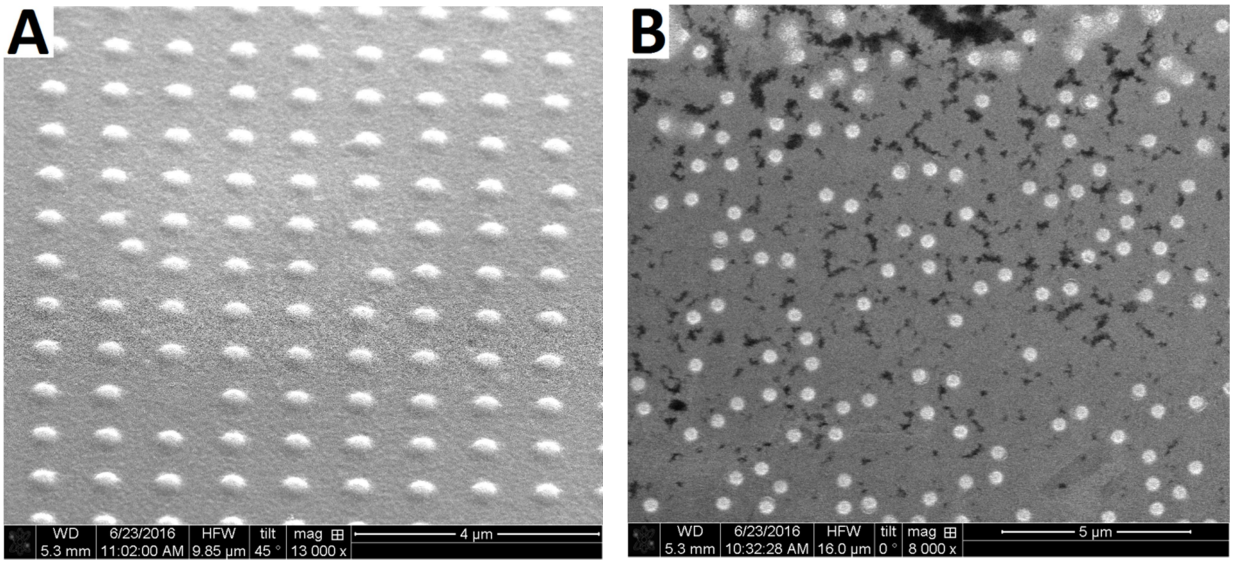

Figure 45: Overview image of part of the pattern created with the hard mask method. A) An overview of the 395 nm pillars. B) An overview of the 395 nm pillars, also the extend of the attachment problem of the resist can be seen.